

From intentions to actions: Neural oscillations encode motor processes through phase, amplitude and phase-amplitude coupling

Etienne Combrisson^{a,b,c,*}, Marcela Perrone-Bertolotti^{d,e}, Juan LP Soto^f, Golnoush Alamian^a, Philippe Kahane^g, Jean-Philippe Lachaux^c, Aymeric Guillot^b, Karim Jerbi^a

^a Psychology Department, University of Montreal, QC, Canada

^b University Claude Bernard Lyon 1, Inter-University Laboratory of Human Movement Biology, 27-29 Boulevard du 11 Novembre 1918, F-69622, Villeurbanne cedex, France

^c Lyon Neuroscience Research Center, Brain Dynamics and Cognition, INSERM U1028, UMR 5292, Lyon University, France

^d Univ. Grenoble Alpes, LPNC, F-38040 Grenoble, France

^e CNRS, LPNC UMR 5105, F-38040 Grenoble, France

^f Telecommunications and Control Engineering Department, University of Sao Paulo, Sao Paulo, Brazil

^g Neurology Dept and GIN U836 INSERM-UJF-CEA, Grenoble University Hospital, Grenoble, France

ARTICLE INFO

Keywords:

Neural oscillations
Intracranial EEG
Motor intention
Motor planning
Phase
Phase-amplitude coupling

ABSTRACT

Goal-directed motor behavior is associated with changes in patterns of rhythmic neuronal activity across widely distributed brain areas. In particular, movement initiation and execution are mediated by patterns of synchronization and desynchronization that occur concurrently across distinct frequency bands and across multiple motor cortical areas. To date, motor-related local oscillatory modulations have been predominantly examined by quantifying increases or suppressions in spectral power. However, beyond signal power, spectral properties such as phase and phase-amplitude coupling (PAC) have also been shown to carry information with regards to the oscillatory dynamics underlying motor processes. Yet, the distinct functional roles of phase, amplitude and PAC across the planning and execution of goal-directed motor behavior remain largely elusive. Here, we address this question with unprecedented resolution thanks to multi-site intracerebral EEG recordings in human subjects while they performed a delayed motor task. To compare the roles of phase, amplitude and PAC, we monitored intracranial brain signals from 748 sites across six medically intractable epilepsy patients at movement execution, and during the delay period where motor intention is present but execution is withheld. In particular, we used a machine-learning framework to identify the key contributions of various neuronal responses. We found a high degree of overlap between brain network patterns observed during planning and those present during execution. Prominent amplitude increases in the delta (2–4 Hz) and high gamma (60–200 Hz) bands were observed during both planning and execution. In contrast, motor alpha (8–13 Hz) and beta (13–30 Hz) power were suppressed during execution, but enhanced during the delay period. Interestingly, single-trial classification revealed that low-frequency phase information, rather than spectral power change, was the most discriminant feature in dissociating action from intention. Additionally, despite providing weaker decoding, PAC features led to statistically significant classification of motor states, particularly in anterior cingulate cortex and premotor brain areas. These results advance our understanding of the distinct and partly overlapping involvement of phase, amplitude and the coupling between them, in the neuronal mechanisms underlying motor intentions and executions.

1. Introduction

The simple motor act of stretching out your arm to grab a cup of coffee is mediated by a rich and complex chain of neuronal processes. What, in essence, may seem as the execution of a straightforward motor command is, in fact, carried out by a cascade of events ranging

from action selection and planning, to motor execution and monitoring. The neural mechanisms that mediate the transformation of a person's intentions into actions have been the subject of a thriving body of research for decades (Ariani et al., 2015; Brovelli et al., 2005; Desmurget and Sirigu, 2009; Jeannerod, 1994; Kalaska, 2009; Lau, 2004; Paus, 2001; Schwartz, 2016; Snyder et al., 1997). However,

* Correspondence to: Psychology Department University of Montreal, Pavillon Marie-Victorin 90, avenue Vincent d'Indy, Quebec, Canada.
E-mail address: e.combrisson@gmail.com (E. Combrisson).

Table 1

Patient data: handedness, age, gender, and description of epilepsy type, etiology, as determined by the clinical staff of the Grenoble Neurological Hospital, Grenoble, France. The lesions (if any were observed) were determined based on the T1 images. Recording sites with epileptogenic activity were excluded from the analyses.

	Handedness	Age	Gender	Epilepsy type	Etiology	EZ localization	Lesion
P1	R	19	F	Frontal	Secondary	Precentral gyrus (RH)	Dysplasia
P2	R	23	F	Frontal	Cryptogenic	Precentral gyrus (LH)	Absent
P3	R	18	F	Frontal	Cryptogenic	Fronto-basal (RH)	Absent
P4	R	18	F	Frontal	Idiopathic	Fronto-central (RH)	Absent
P5	R	31	F	Insula	Secondary	Operculum (RH)	Cavernoma
P6	R	24	F	Frontal	Secondary	Supra-sylvian posterior (LH)	Vascular sequelae

because the neuronal processes at play can be observed at various spatial scales, and with different recording techniques, parallel streams of research have given rise to a rich but fragmented understanding of the local and large-scale integrative electrophysiological mechanisms that are involved in motor control.

Both human and non-human primate research provides solid evidence that goal-directed motor behavior is associated with changes in the patterns of rhythmic neuronal activity across largely distributed brain areas (Schnitzler and Gross, 2005). Movement initiation and execution are mediated by patterns of synchronization and desynchronization that occur concurrently across distinct frequency bands and within multiple motor cortical areas (Cheyne et al., 2008; Jurkiewicz et al., 2006; Pfurtscheller et al., 2003; Saleh et al., 2010).

To date, motor-related local oscillatory modulations are by and large examined by quantifying increases or suppressions in spectral power (Cheyne et al., 2008; Jurkiewicz et al., 2006; Pfurtscheller et al., 2003; Saleh et al., 2010). However, beyond band-limited oscillatory power, other spectral properties, namely phase and phase-amplitude coupling (PAC), are also thought to play a key role in neuronal encoding and information processing. The involvement of phase information in neuronal encoding has been extensively investigated in numerous perceptual modalities and higher-order cognitive tasks (Drewes and VanRullen, 2011; Dugue et al., 2011; Jensen et al., 2014; Klimesch et al., 2008, 2007; Montemurro et al., 2008; Palva and Palva, 2007; Sauseng and Klimesch, 2008; Sherman et al., 2016; VanRullen et al., 2011). In comparison, the role of phase and phase-based measures mediating motor processes are still insufficiently studied. Interestingly, a few studies provide evidence for the involvement of low-frequency phase and amplitude in the neuronal encoding of movement features (Hammer et al., 2016, 2013; Jerbi et al., 2011, 2007; Milekovic et al., 2012; Miller et al., 2012; Waldert et al., 2009, 2008). Nevertheless, the spatial, temporal and spectral dynamics of putative phase coding in the chain of processes are still largely unresolved: starting from goal encoding, to motor planning and motor command execution.

Recent years have witnessed a surge in interest in the putative mechanistic function of PAC (Cohen et al., 2008; Hemptinne et al., 2013; Lee and Jeong, 2013; Newman et al., 2013; Voytek, 2010; Bahramisharif et al., 2013), and numerous measures of PAC have been proposed (Canolty, 2006; Nakhnikian et al., 2016; Tort et al., 2010; Voytek et al., 2013, Özkurt, 2012). Conceptually, PAC may provide a flexible framework for information processing by means of cross-frequency synchronization (Canolty and Knight, 2010; Hyafil et al., 2015; Maris et al., 2011; Staresina et al., 2015; van der Meij et al., 2012; Weaver et al., 2016). However, despite important advances (Hemptinne et al., 2013; Özkurt and Schnitzler, 2011; Soto and Jerbi, 2012; Yanagisawa et al., 2012), the precise role of PAC in mediating motor planning and execution is not yet fully resolved. Specifically, the distinct functional roles of phase, amplitude and PAC estimates during motor behavior remain generally ill-defined.

In the present paper, we compare the involvement of all three of these features using multi-site intracerebral depth electrode recordings from human subjects performing a delayed motor task. Using high spatial, spectral and temporal resolution, we monitored modulations of

neuronal activity, not only at movement execution but, also, during the delay time-window when motor intention is present but execution is withheld. In addition to standard statistical comparisons, we used a single-trial classification procedure (supervised learning) to identify the key contributions of three distinct oscillatory features (phase, amplitude and PAC) to the various motor-related processes along the chain of processes, from goal encoding to movement execution.

2. Material and methods

2.1. Participants

Six patients with medically intractable epilepsy participated in this study (6 females, mean age 22.17 ± 4.6). The patients were stereotactically implanted with multi-lead EEG depth electrodes at the Epilepsy Department of the Grenoble Neurological Hospital (Grenoble, France). In collaboration with the medical staff, and based on visual inspection, electrodes presenting pathological waveforms were discarded from the present study. All participants provided written informed consent, and the experimental procedures were approved by the Institutional Review Board, as well as by the National French Science Ethical Committee. Patient-specific clinical details can be found in Table 1.

2.2. Electrode implantation and stereotactic EEG recordings

Each patient was implanted with stereotactic electroencephalography (SEEG) electrodes. Each one of these had a diameter of 0.8 mm and, depending on the implanted structure, was composed of 10 to 15 contacts that were 2 mm wide and 1.5 mm apart (DIXI Medical Instrument). Intracranial EEG signals were recorded from a total of 748 intracerebral sites across all patients (126 sites in each participant, except for one patient who had 118 recording sites). At the time of acquisition, a white matter electrode was used as reference, and data was bandpass filtered from 0.1 to 200 Hz and sampled at 1024 Hz. Electrode locations were determined using the stereotactic implantation scheme and the Talairach and Tournoux proportional atlas (Talairach and Tournoux, 1993). The electrodes were localized in each individual subject in Talairach coordinates (based on post-implantation CT), and then transformed to standard MNI coordinate system according to standard routines and previously reported procedures (Bastin et al., 2016; Jerbi et al., 2010, 2009; Ossandon et al., 2011).

2.3. Delayed center-out motor task

After a rest period of 1000 ms, the participants were visually cued to prepare a movement towards a target in one of four possible directions: up, down, left or right (*Planning phase*). Next, after a 1500 ms delay period, a Go signal prompted the subjects to move the cursor towards the target (*Execution phase*). The Go signal consisted of a central cue changing from white to black. Fig. 1B shows the task design.

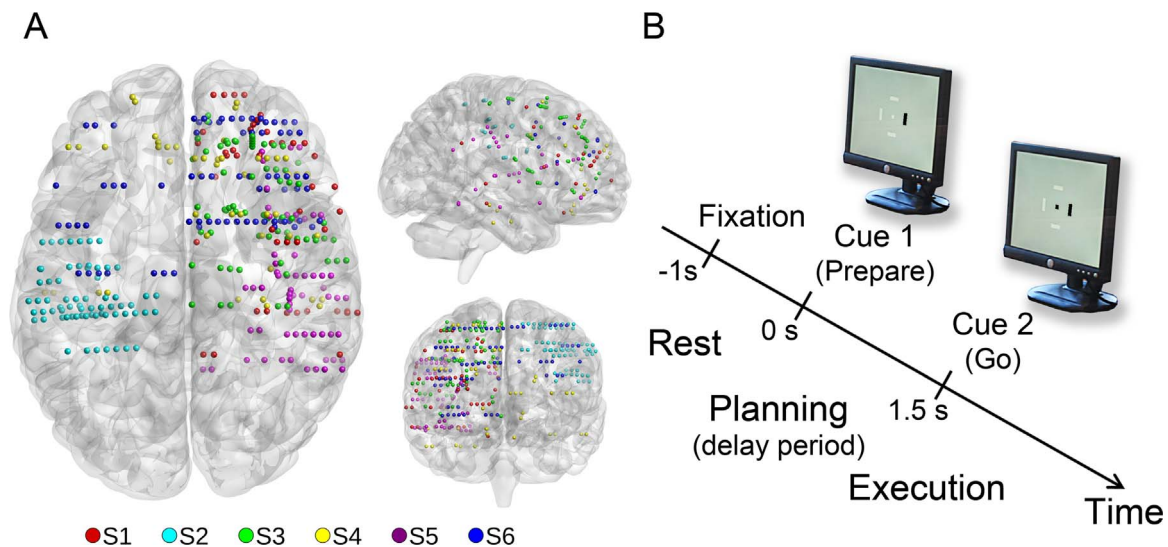


Fig. 1. Implantation visualization for the 6 subjects on a 3-D standard (MNI) brain, and the delayed center-out task definition. (A) Depth electrodes representation from top, right and frontal views. Each subject is associated to a different color. (B) Design of the delayed motor task, where the direction of the movement was instructed at Cue1, and the actual movement was carried out at Cue 2 (“Go signal”). The timeline consisted of three periods: rest, a delay period (motor planning/intention), and movement execution. (For interpretation of the references to color in this figure legend, the reader is referred to the web version of this article.)

2.4. Data preprocessing

SEEG data preprocessing was conducted according to our routine procedures (Bastin et al., 2016; Jerbi et al., 2009). These included signal bipolarization, where each electrode site was re-referenced to its direct neighbor. Bipolar re-referencing can increase sensitivity and reduce artefacts by canceling out distant signals that are picked up by adjacent electrode contacts (e.g. mains power). The spatial resolution of bipolar SEEG of our electrodes were approximately 3 mm (Jerbi et al., 2009; Kahane et al., 2006; Lachaux et al., 2003). Next, using visual inspection and time-frequency explorations of the signal, we excluded electrodes containing pathological epileptic activity. In addition, electrodes located close to the extra-ocular eye muscles were systematically excluded to avoid eye-movement contaminations in our analyses. The pre-processing led to a total of 580 bipolar derivations across all participants (The distribution of all electrode sites across subjects and Brodmann Areas are provided in [Supplementary Fig. S1](#)).

2.5. Spectral analyses

We investigated phase, power, and phase-amplitude coupling in several standard frequency bands defined as follows: very low frequency component (VLFC) [0.1–1.5 Hz], delta (δ) [2–4 Hz], theta (θ) [5–7 Hz], alpha (α) [8–13 Hz], beta (β) [13–30 Hz], low-gamma (low γ) [30–60] and broadband gamma (high γ) [60–200 Hz]. The power features were computed in six bands (δ , θ , α , β , low γ and high γ), the phase features were extracted for 4 bands (VLFC, δ , θ and α), and the phase-amplitude coupling was extracted using three combinations (δ , θ and α for phase and high γ for amplitude). In total, 13 features were extracted for each SEEG bipolar derivation. [Fig. 2](#) illustrates time and frequency-domain features extracted from an illustrative iEEG signal in premotor cortex (BA6).

2.5.1. Spectral power estimation

Band-specific power modulations were computed using the Hilbert transform. To this end, and to avoid phase shifting, we first filtered the data in the required band using a two-way zero-phase lag finite impulse response (FIR) Least-Squares filter implemented in the EEGLAB toolbox (Delorme and Makeig, 2004). This filter has been used in several studies where preserving phase is critical (e.g. Kramer et al., 2008; Cohen et al., 2008; Voytek et al., 2013; Yanagisawa et al., 2012).

Next, we computed the Hilbert transform of the filtered signal and calculated power by taking the square of the amplitude component (envelope). For the specific case of high-gamma power, we split the 60–200 Hz range into multiple, non-overlapping, 10 Hz bands. As in our previous studies (Hamamé et al., 2014; Perrone-Bertolotti et al., 2012; Vidal et al., 2014, 2012), broadband gamma power was obtained by taking the mean of all of the successive 10 Hz wide normalized bands (Jerbi et al., 2009; Ossandon et al., 2011, Bastin et al., 2016). Although comparable power estimations were obtained using Morlet wavelets (e.g. Tallon-Baudry et al., 1996), we chose to use the Hilbert-based power computation to have a homogeneous methodological framework across all three features, as the Hilbert method was used to assess phase and PAC features (see below).

2.5.1.1. Rationale for broadband gamma selection. Motor-related power modulations in the gamma-band have been observed with intracranial recordings across a wide range of frequencies extending up to 180 Hz or 200 Hz (e.g. Leuthardt et al., 2004; Crone et al., 2006; Miller et al., 2007). Yet, there is also ample evidence in the literature for prominent motor gamma oscillations within a narrower 60–90 Hz band, often with peaks around 75 or 80 Hz (e.g. Ball et al., 2008; Cheyne et al., 2008; Muthukumaraswamy, 2010, 2011; Jenkinson et al., 2013). Because many of these studies were conducted with EEG or MEG, one might argue that this discrepancy can in part be a reflection of differences between invasive and non-invasive gamma investigations. Electrophysiological recordings in non-human primates have demonstrated that changes in narrow-band gamma oscillations and in broadband gamma activity can occur simultaneously and that they are likely to reflect distinct phenomena (Ray and Maunsell, 2011). We chose to subdivide the gamma band into low gamma (30–60 Hz) and broadband gamma (60–200 Hz) in part because the latter band facilitated comparisons of our power results with our PAC findings, as well as with wide-band gamma power results in the intracranial EEG literature.

Note that for visualization purposes, cortical mapping of significant power modulations on the standard MNI brain (e.g. [Figs. 3–5](#)) was done after normalization with respect to a baseline window of 500 ms during pre-stimulus rest (from –750 ms to –250 ms). The power in each frequency band was normalized by computing the relative change compared to this baseline at the same frequency (i.e. subtracting and

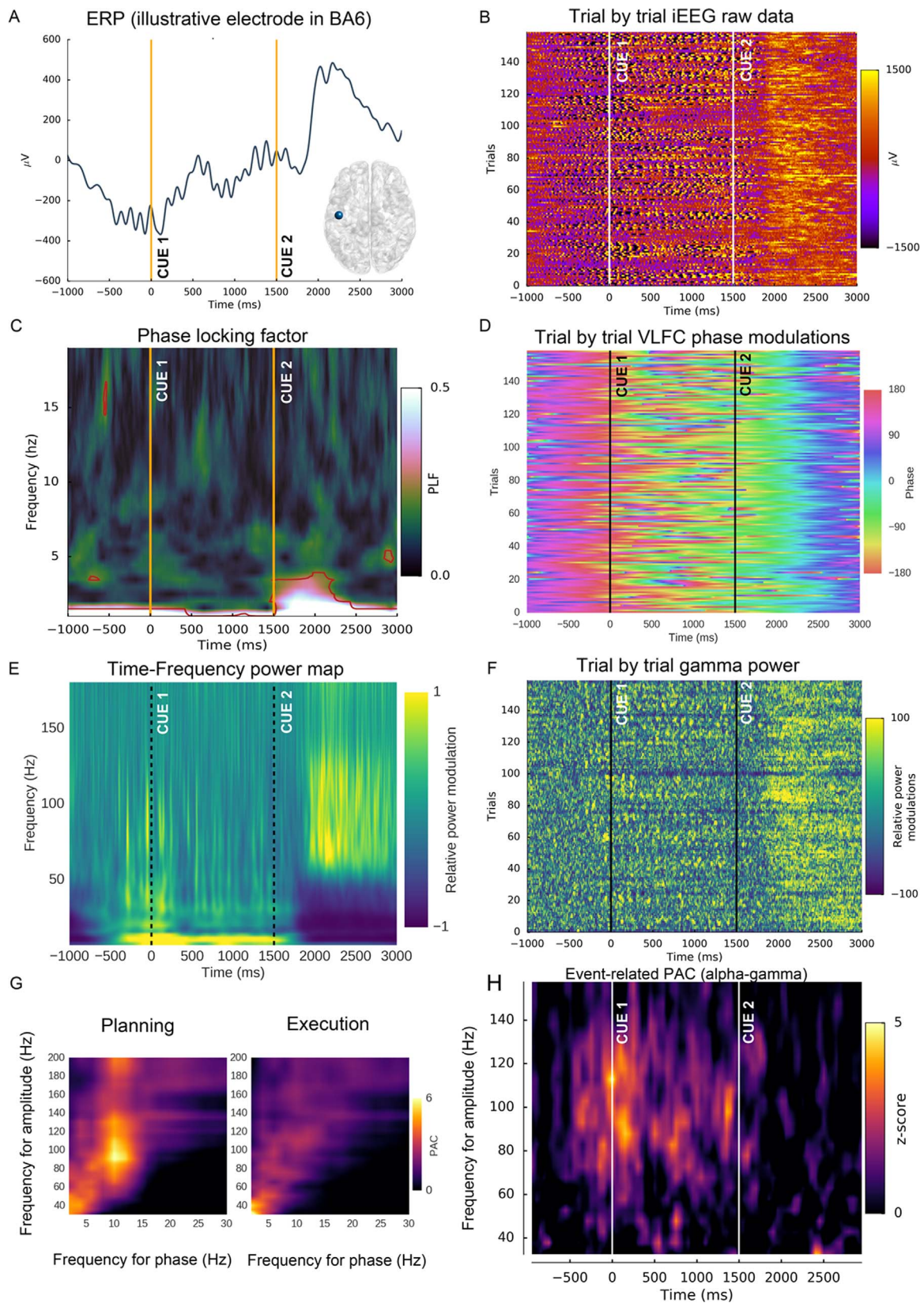


Fig. 2. Oscillatory feature extractions from intracranial EEG (iEEG) signals shown for an illustrative electrode in human premotor cortex (BA6). (A) Event-related potential (ERP) across the experiment timeline and anatomical location of the electrode. (B) Trial-by-trial raw iEEG signals. (C) Phase-locking factor indicating stimulus phase-locking (D) Single-trial phase shown for the VLFC (< 1.5 Hz) frequency range. (E) Time-Frequency representation. (F) Trial-by-trial broadband gamma power (60–200 Hz). (G) Phase-amplitude coupling maps during planning and execution, revealing prominent alpha-gamma coupling present during planning that was absent during execution. (H) Event-related PAC depicts, for the same electrode, the time course of alpha-gamma PAC.

dividing by the mean of the baseline).

2.5.1.2. Statistical evaluation of tasked-based power modulations. Significant power modulations were obtained by standard two-tailed permutation tests, where power values (across time and frequency) during the task were randomly permuted with the corresponding value during baseline. A total of 1000 permutations were performed yielding a null distribution for the relative power, providing a minimal p -value of 0.001.

2.5.1.3. Power-based classification. The power features used for classification were computed as mean power over 500 ms time windows during planning (250 to 750 ms), execution (2000 to 2500 ms) and (−750, −250 ms) during pre-stimulus rest, where $t=0$ ms corresponds to the onset of Cue 1. Note that when decoding “Exec vs Intention” (Fig. 6C), the single-trial power features used were first baseline normalized (with respect to the rest period) on a trial-by-trial basis. However, no such baseline-based feature normalization was possible when running classifications where the rest window was itself one of the classes (i.e. “Exec vs Rest”, “Intention vs Rest” and the 3-class decoding “Exec vs Intention vs Rest”, Fig. 6 panels A, B and D). While decoding results with and without baseline normalized features (for Execution vs Intention) were very similar, the normalized features appeared to provide more reliable decoding. This could be in part due to a beneficial effect of feature normalization on classifier performance.

2.5.2. Phase estimation

To extract phase features in a given frequency band, we first applied a bandpass filter to the bipolarized signals. Next, we extracted the angle of the complex time-series based on the Hilbert transform. This gave the instantaneous phase for all time points. Phase was extracted using the same type of filter as the one used to extract spectral power.

2.5.2.1. Statistical evaluation of tasked-based phase modulations. we used Rayleigh’s test to compute significant phase modulations (Babiloni et al., 2002; Lakatos, 2005; Tallon-Baudry et al., 1996), using the circular statistics toolbox (Berens et al., 2009).

2.5.2.2. Phase-based classification. For decoding purposes, we considered instantaneous phase features at −500 ms for rest, 500 ms for planning and 2250 ms for execution. These time points were chosen because they correspond to the center of each time window used for power estimation.

2.5.3. Phase-Amplitude Coupling (PAC) estimation

Different methods for the estimation of PAC have been used in the literature (Jensen and Colgin, 2007; Canolty and Knight, 2010; Tort et al., 2010; Soto and Jerbi, 2012; Aru et al., 2015). In order to choose which method to apply here, we simulated synthetic PAC signals (e.g. Tort et al., 2010), and tested the behavior of several methods, namely Mean Vector Length (MVL) (Canolty, 2006), the Height-Ratio (HR) (Lakatos, 2005), Kullback-Leiber divergence (Tort et al., 2010), and normalized direct PAC (ndPAC) (Özkurt, 2012). We found that the tested PAC methods provided very comparable results. The slight differences arose from applying different normalization or surrogate procedures to the data. Based on this finding, we chose to use the MVL method combined with a normalization method, where the surrogate values were calculated by randomly swapping phase and amplitude across trials (cf. Tort et al., 2010). In short, the PAC estimation procedure that was applied can be summarized as follows. First, low-frequency phase and high-frequency amplitude signals were obtained

by filtering and applying Hilbert transformation in the frequencies of interest (Canolty, 2006). Being frequency-dependent, the optimal filter orders were adapted separately for the phase of the slower oscillations (3 cycles used), and for the amplitude of the faster oscillations (6 cycles), as proposed in previous studies (e.g. Bahramisharif et al., 2013). Next, surrogate data were generated by randomly swapping the phase trial data and amplitude trial data (i.e. randomly association of the high frequency amplitude envelope of a trial with the low-frequency phase time course of another trial). This procedure was repeated 1000 times. Finally, the normalized PAC value was obtained by normalizing the MVL by the surrogate data, yielding a z-score. This procedure is in line with previous PAC studies (Canolty, 2006). This form of statistical normalization using surrogate data provides a more robust estimate than non-normalized measures (Özkurt and Schnitzler, 2011).

To visualize the emergence of PAC, we used a combination of methods: (a) phase-alignment of single-trial time-frequency maps (Canolty, 2006; Hemptinne et al., 2013), (b) a comodulogram (e.g. Foster and Parvizi, 2012; Pittman-Polletta et al., 2014), and (c) event related phase-amplitude coupling (Voytek et al., 2013). When computing the comodulogram, we used the entire planning and execution periods (1500 ms for each) in order to maximize the per-trial number of oscillation cycles for the estimation of PAC.

2.5.3.1. Statistical evaluation of tasked-based PAC modulations. The statistical assessment of PAC was achieved by comparing the true PAC values to the null distribution of PAC values, computed using surrogate data (i.e. random shuffling across trials of phase and amplitude signals, Tort et al. 2010). A real PAC value, which was higher than the 999th highest PAC value obtained with surrogate data, was considered significant at $p < 0.001$.

2.5.3.2. PAC-based classification. For decoding, we used the normalized PAC values computed over the entire window of each condition; in other words [−1000, 0 ms] for Rest, [0, 1500 ms] for planning and [1500, 3000 ms] for execution. Note here, that by normalization, we refer to the transformation to z-scores based on surrogate data, not normalization with regards to pre-stimulus baseline levels.

2.6. Signal classification

We set out to explore the feasibility of using multi-site human Local Field Potential (LFP) data (580 bipolar electrode sites) to perform three types of motor-state classifications: (a) Execution vs Rest, (b) Intention vs Rest, and (c) Execution vs Intention. We compared the performance of several classification algorithms (Linear Discriminant Analysis (LDA), Naïve Bayes (NB), k-th Nearest Neighbor (KNN), Support Vector Machine (SVM) with linear and Radial Basis Function kernels and Random Forest). For single features classification, LDA, NB and SVM all provided similar results. We chose to use the LDA approach for its speed, which was of particular importance given the computationally-demanding permutation tests used to evaluate classifier performance.

2.7. Decoding accuracy and statistical evaluation of decoding performance

Classification performance was evaluated using standard stratified 10-fold cross-validation. First, the data set was pseudo-randomly split into 10, equally-sized, observations: 9 segments were used for training the classifier, and the last one as the test set. This procedure was repeated 10 times, such that every observation in the data was used exactly once for testing, and at least once for training, but never at the

same time. This strict separation of training and testing was critical to ensure the test data was naïve and did not violate basic classification principles (Lemm et al., 2011). The use of stratification seeks to ensure that the relative proportion of labels (or classes) in the whole data set is reasonably preserved within each of the segments after the split. The above procedure was repeated 10 times to reduce the effect of the random generation of folds, yielding a 10 times 10-fold cross-validation framework. Next, the performance of the achieved decoding was calculated using the decoding accuracy (DA) metric, which was computed as the mean correct classification across all folds. Although the use of theoretical chance-levels (e.g. DA=50% for binary classification) can provide some useful indication on classifier performance in the presence of a high number of observations, the use of statistics is mandatory in order to assess the significance of classification performance (Combrisson and Jerbi, 2015). To this end, we used a permutation testing framework where the cross-validation and DA calculations were recomputed after randomly shuffling the labels of the classes. For each site and for each type of feature (i.e. power, phase and phase-amplitude coupling), 1000 permutations were generated, thus allowing for statistical assessments with p values as low as 0.001 (Combrisson and Jerbi, 2015; Ojala and Garriga, 2010, Golland and Fischl, 2003; Meyers and Kreiman, 2012).

2.8. Data mapping to a 3-D standard cortical representation

To facilitate the interpretation of the results, all significant task-based feature modulations and decoding results were remapped from the intracranial electrode sites onto a standard cortical representation. To achieve this, all electrode coordinates were transformed from individual Talairach space to standard MNI space, and custom Matlab code was written to project the data from SEEG sites onto the cortical surface. In practice, data from the iEEG electrodes were assigned to the vertices on the MNI cortical mesh that fell within a fixed radial distance of 10 mm from each electrode. This cortical representation technique is methodologically consistent with methods used in previous iEEG studies (Bastin et al., 2016; Jerbi et al., 2009; Ossandon et al., 2012). In addition to generating brain-wide visualization of all significant features and decoding performances, this method was also used to display the cortical coverage provided by all the electrodes in this study (dark gray areas in Fig. 2A). Note that, by convention, the left hemisphere (LH) is presented on the left in all brain visualizations (Figs. 3 to 5). Furthermore, these 3D cortical maps of task-based feature modulations only show contralateral effects; if the patients were implanted in the left hemisphere (LH), we used data obtained using the right hand and vice versa. For the two patients who were implanted bilaterally we kept the right hemisphere (RH) electrode data when analyzing left hand movements, and the LH electrodes for analysis of right hand movements.

3. Results

The frequency domain analysis of the 580 intracranial bipolar recordings across all participants revealed that the delayed motor task was mediated by complex patterns of spectral modulations across widely distributed brain areas. Fig. 2 illustrates task-related modulations of amplitude, phase and phase-amplitude coupling measured by a recording site in premotor cortex (BA6) in one participant. The ERP and single-trial raw iEEG recordings for this electrode are shown in panels 2A and 2B, respectively. Panels 2C and 2D depict the phase-locking factor and a trial-by-trial phase representation across time. The illustrative time-frequency map (Fig. 2E) depicts a typical power modulation pattern, where movement execution was associated with a strong increase in broadband gamma power, and simultaneous power suppression in the alpha, beta and low-gamma frequency bands. The delay period (between Cue1 and Cue2) at this site showed a different pattern of power increases at slow frequencies in the delta to alpha

range. Because of the high signal-to-noise ratio (SNR) of the intracranial EEG recordings used, it is possible to estimate broadband gamma (60–200 Hz) power on a trial-by-trial basis (Fig. 2F). The PAC maps in Fig. 2G illustrate the changes in PAC values for the same recording site across motor planning and execution. A peak in PAC between alpha phase and high gamma amplitude was observed during the pre-movement delay period, this feature vanishes during execution, when the maximum PAC was observed between delta phase and low-gamma amplitude. The predominance of the alpha-gamma coupling in the delay period was also confirmed when the time-frequency (TF) maps were computed by realigning the single-trial TF maps to alpha phase in the vicinity of the cue (results not shown). Finally, time-resolved, event-related, PAC estimations (Fig. 2H) revealed the existence of an alpha-gamma coupling specific to the delay period. These oscillatory feature estimations were primarily presented as an illustration of the wide variety and high SNR of the features explored in this study, using averaging over trials and, most importantly, in trial-by-trial mode. In the following section, we discuss the global results obtained using data from all participants. First, we describe the task-based oscillatory modulations, and then we examine the results of the data-mining approach.

3.1. Task-based Spectral power modulations

The cortical mapping of power modulations during the delay period and motor execution reveal distinct patterns of increases and decreases across the various frequency bands (Fig. 3). As one would expect from previous, invasive, reports in humans (Crone et al., 1998; Crone et al., 2006; Babiloni et al., 2016; Bundy et al., 2016; Rektor et al., 2006), our results confirmed that motor execution is associated with prominent suppressions of alpha/mu and beta band powers, and with increases in high gamma power, primarily in motor and premotor cortices. Moreover, the power modulations shown in Fig. 3 are indicative of significant task-based modulations beyond these areas, extending to parietal, prefrontal and cingulate areas. When comparing the brain-wide significant power changes for both planning and execution, we first observed a large degree of overlap between the statistically significantly active areas in both conditions. Second, two distinct patterns appeared to emerge when we examined the direction of the effects across frequency bands: the alpha, beta and low-gamma bands showed a reversal of the effect, from a significant increase during planning to a significant suppression during execution. By contrast, the remaining bands (delta, theta and high gamma) displayed a consistent significant power increase during both the planning and execution periods, with a stronger effect at the execution of the movement. Of note, high-gamma increases were prominent over multiple frontal and prefrontal brain areas bilaterally, with strong peaks in motor and premotor cortices during execution. Most of these areas also showed a significant increase of power above baseline levels during the delay period, potentially related to movement goal-encoding and motor planning processes.

3.2. Task-based phase modulations

The patterns of statistically significant changes in phase revealed a predominant effect in the lower frequencies (Fig. 4). In particular, the VLFC range (i.e. < 1.5 Hz) showed consistent phase values in primary motor cortex (with a reversal in sign between planning and execution, at the given time instants). Interestingly, although less prominent, consistent phase effects were also found in the theta and alpha bands, predominantly in prefrontal areas. The significant delta phase angle over primary motor cortex during execution is in line with earlier reports on delta-range coherence between motor cortex and movement parameters (Jerbi et al., 2007).

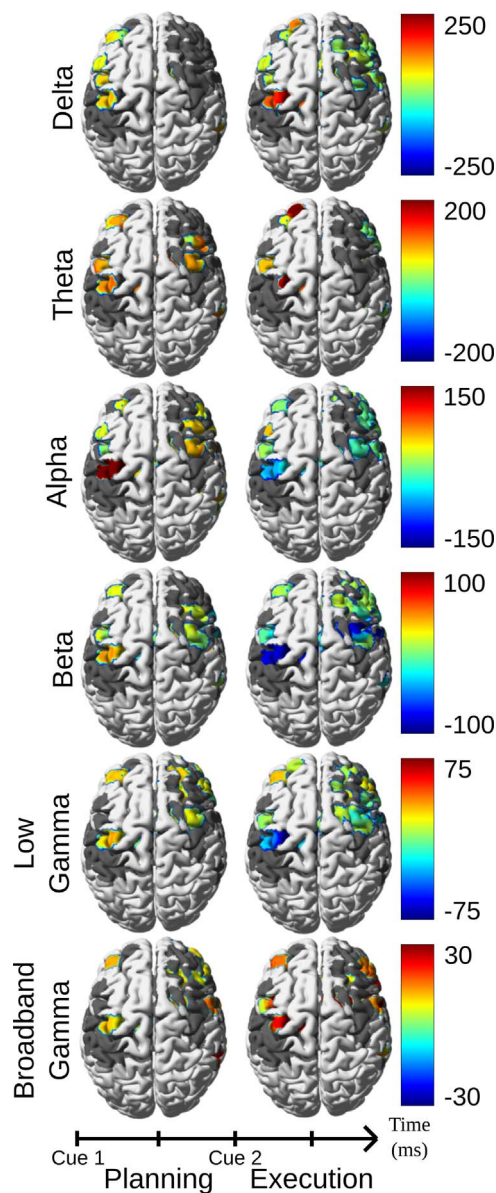


Fig. 3. Task-related modulations of spectral power during planning and execution of upper limb movements. The color bars represent percent relative changes (%) of power during planning (250–750 ms) and during execution (2000–2500 ms), with respect to baseline power during pre-stimulus rest (–750 to –250 ms). The power modulations are shown for delta (2–4 Hz), theta (5–7 Hz), alpha (8–13 Hz), beta (13–30 Hz), low-gamma (30–60 Hz) and broadband gamma (60–200 Hz). All modulations shown were statistically significant (permutation tests, $p < 0.05$, FDR-corrected). Dark gray areas represent cortical regions for which electrode coverage was available but, where the modulations did not reach statistical significance. By convention, the left hemisphere (LH) is presented on the left.

3.3. Task-based PAC modulations

Statistically significant levels of phase-amplitude coupling were observed in multiple brain areas and with very similar distributions at execution, and during the delay period in the absence of movement (Fig. 5). In fact, our results suggest higher PAC during the goal-encoding and planning phase than during movement execution. The most prominent PAC effects in primary motor cortex were obtained for alpha-gamma interactions, but were only present during the planning period. This alpha-gamma PAC in primary motor cortex (M1) virtually disappeared at the time of execution. Interestingly, it was replaced by an M1 delta-gamma PAC during motor execution. In addition, as shown in the right panel of Fig. 5, depth recordings in the medial wall

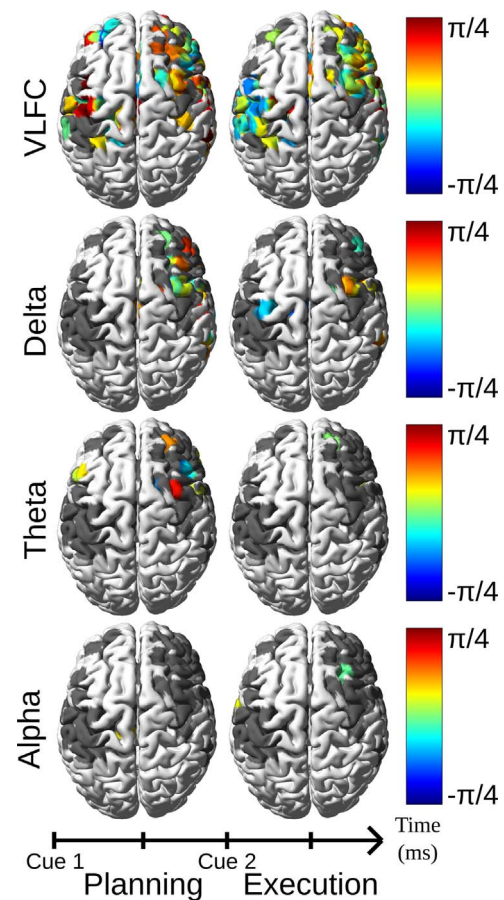


Fig. 4. Task-related modulations of instantaneous phase during planning and execution of upper limb movements. The color bars represent mean phase computed at 500 ms (planning) and at 2250 ms (execution), which corresponds to the centers of the windows used for power (Fig. 3). Phase modulations were computed for very low frequency component (VLFC) (< 1.5 Hz), delta (2–4 Hz), theta (5–7 Hz) and alpha (8–13 Hz) bands. All modulations were statistically significant (Rayleigh's test), based on the circular statistics toolbox (Berens et al., 2009), $p < 0.001$. Dark gray areas represent cortical regions for which electrode coverage was available but, where the modulations did not reach statistical significance. By convention, the left hemisphere (LH) is presented on the left.

revealed statistically significant PAC in anterior cingulate cortex (ACC), in particular, cingulate motor cortex (CMA, BA32) and in medial premotor areas, specifically in supplementary motor area (SMA, BA6) for three slow-frequency bands (delta, theta and alpha). These PAC modulations are likely to reflect the involvement of SMA and cingulate motor areas in action selection, planning, execution, and inhibition.

3.4. Single-trial decoding of motor processes using machine learning

The application of a supervised learning framework allowed us to determine which features, among those discussed above, were useful for single-trial decoding of motor states (binary classification applied pairwise to rest, planning and execution states, as well as a three-class decoding of rest, planning and execution). This was achieved using a cross-validation approach in which a classifier was repeatedly trained on a subset of the data and, then, tested on previously unseen single-epoch observations (test set). This method allowed us to quantify the decoding strength of each feature with a percent correct classification rate.

Fig. 6 depicts mean decoding accuracies (DA) achieved with each feature (power, phase, PAC) across all frequency bands, and all Brodmann areas for which recordings were available (The same significant results pooled by feature, but averaged across Brodmann

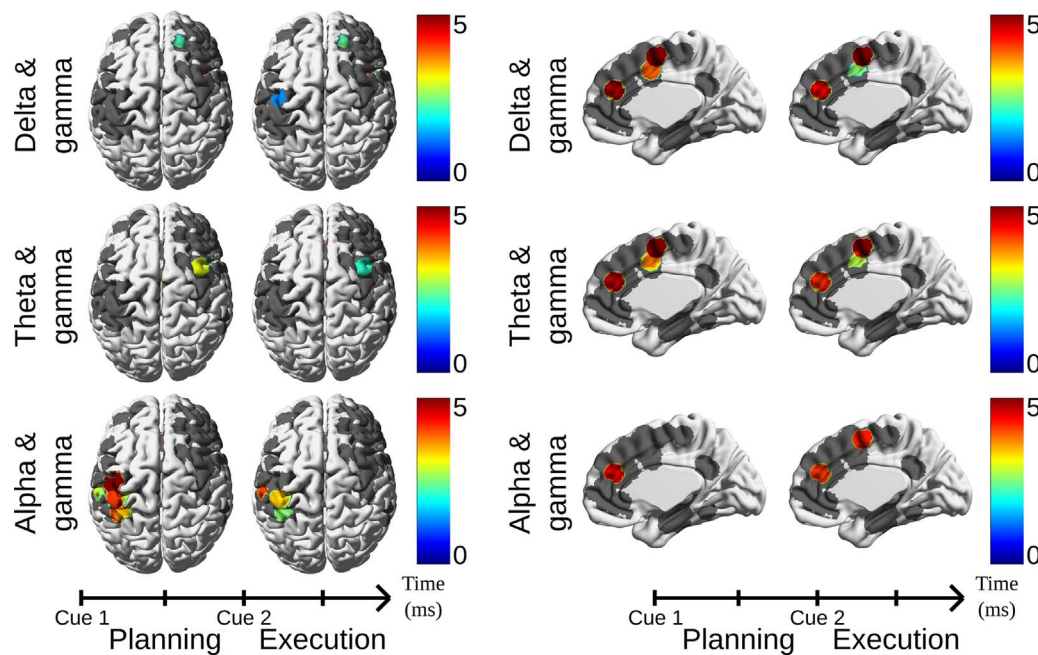


Fig. 5. Task-related modulations of phase-amplitude coupling during planning and execution of upper limb movements (Left panel: top view, Right panel: medial view). The color bars represent mean PAC modulation index (MI), quantifying the co-modulation of broadband gamma amplitude (60–200 Hz) with delta (2–4 Hz), theta (5–7 Hz) and alpha (8–13 Hz) bands. All modulations shown were statistically significant ($p < 0.001$, surrogate data), and are estimated from the entire planning and execution time windows. Dark gray areas represent cortical regions for which electrode coverage was available but, where the modulations did not reach statistical significance. By convention, the left hemisphere (LH) is presented on the left.

areas are available in [Supplementary Fig. S2](#)). The bar plots above each panel depict the highest decoding accuracies obtained with each feature, and the Brodmann area in which it was observed. The bar plots on the right side of each panel indicate the number of significant features present in each Brodmann area. It is noteworthy that all three feature types (amplitude, phase and PAC) computed across many frequencies, and most of the probed brain areas, contained to variable degrees discriminant information on motor states (All results in [Fig. 6](#) represent statistically significant results using permutation tests corrected for multiple comparisons using maximum statistics, $p < 0.05$).

3.4.1. Classification similarities between Execution vs Rest and Intention vs Rest

The highest percentages of correct prediction were obtained when classifying Rest vs. Execution (as high as 94.9% on single-trial classifications). A high degree of similarity was observed between the decoding patterns for Execution vs Rest ([Fig. 6A](#)), and Intention vs Rest ([Fig. 6B](#)). In principle, most of the features that provided significant decoding of Execution vs Rest, also provided significant decoding of Intention vs Rest. The features that yielded the highest discrimination in both cases primarily involved spectral power in beta, low-gamma, and broadband gamma bands, in addition to phase in the very low frequency range (< 1.5 Hz). The most prominent brain areas involved in both types of decoding were BA 4, 6, 8, 9, 13, 32 and 40. These were the regions that contained the highest number of significantly decoding sites (gray histograms), and these were also the BAs that yielded the highest levels of decoding accuracy. The highest DA performances reached 94.9% (VLFC phase in premotor cortex) when decoding Execution vs Rest, and 91.3% (VLFC phase in inferior parietal cortex, BA40) in the case of Intention vs Rest.

3.4.2. Classification differences between Execution vs Rest and Intention vs Rest

Although the decoding matrices in [Fig. 6A](#) (Execution vs Rest) and [6B](#) (Intention vs Rest) show a high degree of similarity, there were also notable differences between the two. First, many more significant sites were obtained in the case of Execution vs Rest (cf. gray bar plots on the

right of each matrix). Furthermore, the low frequency phase in BA 40 played a more central role in distinguishing intention from rest, than movement execution from rest. This could be in line with what is known about the role of the inferior parietal lobe in motor planning ([Caspers et al., 2008](#); [Mattingley et al., 1998](#); [Rushworth et al., 2001](#)). In addition, power-based classification results showed that, while primary motor (BA4) and premotor areas (BA6) were important in predicting execution, the most noticeable intention-decoding power features were recorded from BA9, 13 and 32 (top histogram in Panel [6B](#)). This is consistent with what is reported in the literature on the involvement of BA9 in the processes of working memory, executive planning and behavioral inhibition. Among other things, the important decoding levels in BA13 could be related to the role of insular cortex in motor planning ([Lacourse et al., 2005](#); [Stephan et al., 1995](#)). Remarkably, the best PAC-mediated decoding of Intention vs Rest was obtained with delta-gamma coupling in the dorsal anterior cingulate cortex (dACC, BA32, DA=70,1%). This prominent PAC in ACC is consistent with the role of this brain region in motor inhibition, visuo-patial attention, motor planning and imagery ([Cheyne et al., 2012](#); [Jahanshahi et al., 1995](#); [Paus, 2001](#)). To the best of our knowledge, this is the first report of a motor-related delta-gamma PAC modulation in ACC.

3.4.3. Classification of Execution versus Intention

The decoding matrix of sub-[Fig. 6C](#) shows a markedly different pattern for Execution vs Intention. Because of the similarity between the neuronal responses in both conditions (cf. previous sections), the differences are subtle and, as a result, the decoding performances are lower than those reported for the Execution vs Rest, or Intention vs Rest classifications. In addition, in this comparison, fewer brain areas allowed for statistically significant decoding. Interestingly, among all features, the one that provided the best discrimination between the intention period and the execution period was the phase of the very low frequency range (< 1.5 Hz), which yielded a decoding peak of 88.9% in BA 8. The second best decoding feature was broadband gamma with a decoding that peaked at 83.5% in the posterior insula (BA13). Moreover, the premotor cortex (BA6) appeared to be overall the most

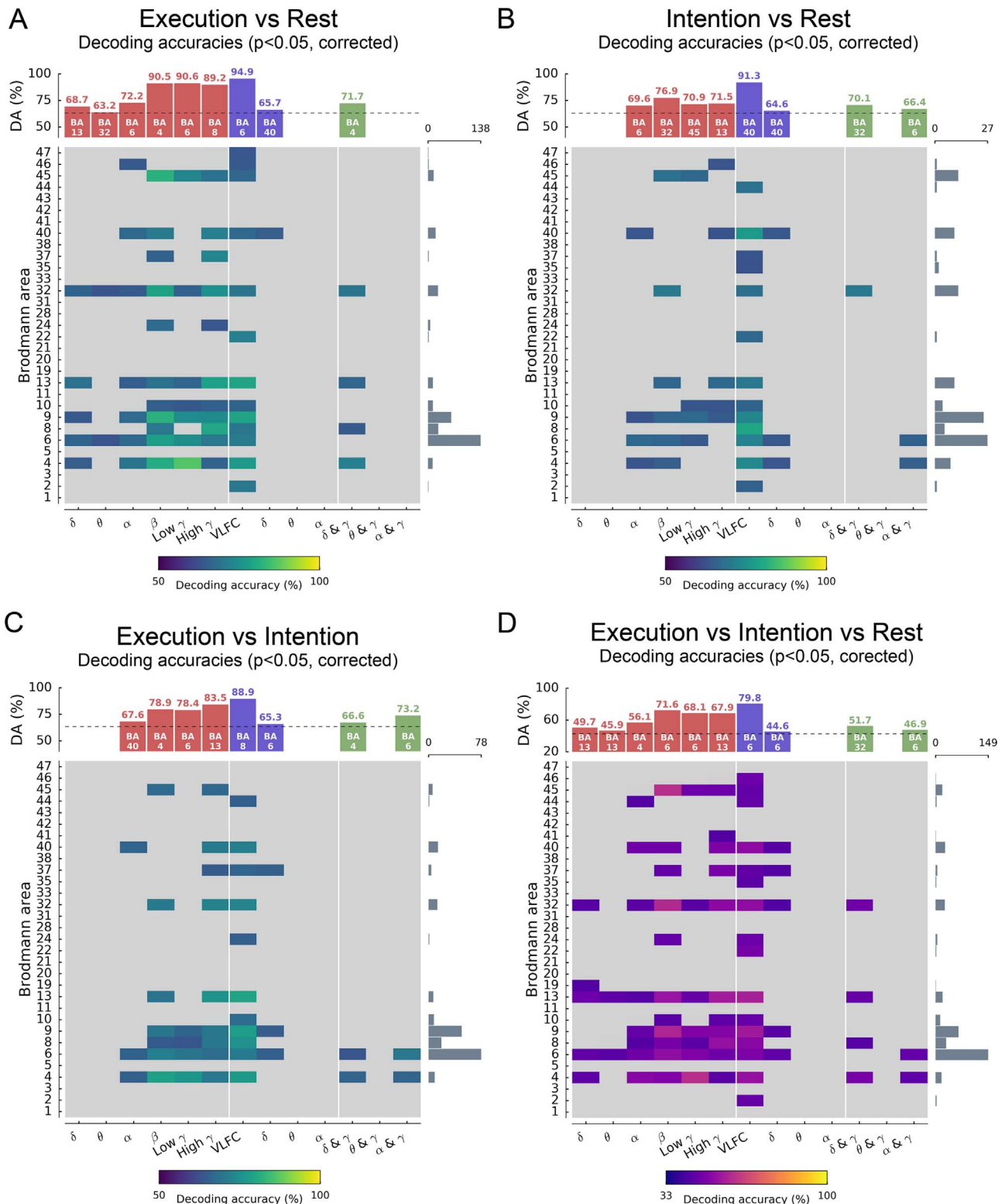


Fig. 6. Single-trial classification of motor states (**pre-stimulus rest, intention and execution**) using the features of power, phase and PAC. **(A)** Execution vs Rest, **(B)** Intention vs Rest **(C)** Execution vs Intention **(D)** Execution vs Intention vs Rest. The decoding matrices depict the mean percent decoding accuracies (DA) for all statistically significant features, across all frequency bands (x-axes) and across all Brodmann Areas in which recordings were available (y-axes). Yellow on the color-bar indicates 100% DA, the lower bounds of the color bars correspond to the chance levels of 50% in the pairwise decoding (A-C) and 33% in the 3-class decoding (D). Only statistically significant decoding accuracies are reported ($p < 0.05$, permutation test, corrected via maximum statistics). The bar plots above each panel show the highest DA obtained with each feature (red: power, blue: phase, and green: PAC), as well as the Brodmann area where it was observed. The gray bar plots on the right side of each panel indicate how many statistically significant features were found in each Brodmann area (note that the upper bounds on the y-axes of these bar plots differ across panels). (For interpretation of the references to color in this figure legend, the reader is referred to the web version of this article.)

prominent area for Execution vs Intention decoding, providing the largest number of statistically significant sites and features. This is in line with the established involvement of the premotor cortex in motor execution, planning and imagery, as well as visuomotor and visuospatial attention (Ball et al., 1999; Gallivan et al., 2013; Hanakawa et al., 2008; Miller et al., 2010). Finally, the data showed that delta-gamma and alpha-gamma provided the best PAC decoding (respectively in BA4 and BA6) cortices (Fig. 6C), while theta-gamma coupling did not provide significant decoding. This finding is best explained by the significant decoding accuracy (in these areas) of delta-gamma and alpha-gamma observed in Execution vs Rest (Fig. 6A) and Intention vs Rest (Fig. 6B), respectively.

3.4.4. Three-class decoding: Execution versus Intention versus Rest

Three-class decoding results (Fig. 6D) provide results that are very similar to those observed in the pair-wise comparisons. The peak decoding was obtained with the VLFC feature in BA6 (79.8%, with a theoretical chance level at 33%). This result confirms the decoding results observed in the pair-wise decoding (Fig. 6A-C). The second and third best results also originate from sites in premotor area (BA6), respectively with the beta and low-gamma power.

4. Discussion

4.1. Summary of findings

Previous reports have reported complex patterns of overlap and segregation between the networks of brain areas involved in action representation, planning and execution (e.g. Jeannerod, 1994; Stephan et al., 1995; Hanakawa et al., 2008; Guillot et al., 2012;) So far, electrophysiological explorations of these patterns in humans have focused on modulations of rhythmic activity, primarily measured through spectral power modulations. Using direct recordings in humans performing a delayed motor task, we provide by the present article an intracranial investigation of the similarities and discrepancies between activations in areas involved in the preparation of action, and those that actually mediate movement execution. To the best of our knowledge, this study provides the first account of these key brain dynamics through a systematic investigation of the roles of phase, amplitude and phase-amplitude coupling across widely distributed brain areas (extending beyond primary motor areas), and across a wide range of frequencies (up to 200 Hz). Furthermore, in addition to statistical comparisons, an important addition of this study was the use of supervised learning and a single-trial classification framework as ways to assess the distinct and overlapping information content of these features.

4.2. Planning and execution are associated with prominent phase, amplitude and PAC modulations

Our analyses of task-based modulations revealed spatially distributed patterns of statistically significant changes in power, phase and PAC, both during the delay period and following the execution cue. Large amounts of overlap were uncovered between the significant modulations observed in the planning processes and those in movement execution. In task-based power changes, significant increases in the delta, theta and broadband gamma bands were present during the planning phase and were further enhanced at the time of execution. By contrast, alpha, beta and low-gamma power showed a rather consistent pattern of inversion, from increases following the preparation cue to decreases following the execution cue. These activation pattern findings in intention and execution echo previously reported similarities and differences between motor imagery and motor execution. In particular, action representation and motor inhibition were likely to be common to, both, the delay period of the task, and to motor imagery tasks (Stephan et al., 1995). Phase and PAC also displayed similar patterns of

responses for action preparation and execution, although they were also indicative of clear discrepancies in motor areas, such as prominent alpha-gamma coupling during planning, but delta-gamma coupling during execution. Although not spatially exhaustive, the reported pre- and peri-movement modulations in power, phase and PAC were observed over large parts of parietal, frontal and prefrontal areas, including medial areas, such as the dACC. Moreover, while the reported power modulations were largely consistent with previous iEEG reports (Crone, 1998; Crone et al., 2006, 1998; Pfurtscheller and Lopes da Silva, 1999), the wide-spread significant modulations of phase and PAC effects during the delay-period and movement execution are, to our knowledge, novel findings that extend the current understanding of their role in mediating motor behavior.

It is noteworthy that the PAC observations reported here are partly consistent with those of an earlier ECoG study (Yanagisawa et al. 2012). By computing cross-frequency coupling in electrodes implanted in motor areas, the authors found that high-gamma amplitude during waiting was strongly coupled with; alpha phase. However, this alpha-gamma PAC was not predictive of movement type and was strongly attenuated towards the timing of motor execution. Similarly, we found prominent motor alpha-gamma PAC during the delay period, which then disappeared during movement execution. Interestingly, in our dataset, the alpha-gamma coupling during the planning was replaced by a delta-gamma coupling at execution. In addition, our data provide evidence for PAC modulations across wider brain areas, beyond primary motor areas.

Future studies might not only benefit from investigating brain activation dynamics through the role of phase, amplitude and phase-amplitude coupling during motor intention and execution, but also during explicit mental simulation of the same movement.

4.3. Decoding patterns reveal functional overlap and discrepancies across phase, amplitude and PAC

The machine learning framework allowed for deeper investigation of the role of our features through the assessment of their decoding accuracy. Most importantly, the classification strategy extended the standard statistical analyses by switching from comparisons of means to the evaluation via cross-validation of the predictive power of the data computed from single-trials; once trained, the classifier was individually applied to each single-trial of the test set. In other words, the mean decoding performances reflected the ability of each feature to discriminate between the conditions (Rest, Intention, Execution) on single samples of data. Taken together, the decoding analyses provide a rich, multi-dimensional, exploration of the functional involvement of phase, amplitude and phase-amplitude in motor behavior. The main findings can be summarized as follows. First, the slow frequency phase achieved the highest DAs across all classifications; Our results revealed its prominent role primarily in inferior parietal areas (DA > 90%). Second, we provide evidence for significant decoding using phase-amplitude coupling in dACC (DA > 70%) during the delay-period preceding motor execution. Third, the performance of power features dropped substantially in the condition Intention vs Rest (below 77%) compared to Execution vs Rest (ca. 90%). During planning, the best power-based decoding levels were observed in prefrontal regions (BA9, 13, 32, 40 and 45), while execution decoding using power revealed strong classifications in BA4, 6, 8 and 9, including precentral and premotor regions. Finally, we showed that when it comes to directly distinguishing the neuronal correlates of execution from those mediating intention, the highest classifications (among all explored regions) were achieved either with the phase of the very low frequency range (< 1.5 Hz) in BA8 (DA > 88%), or with broadband gamma power (60–200 Hz) in the posterior insula (DA > 83%).

4.4. Relationship with previous electrophysiological findings

Overall, the present analysis of intracranial human data provides strong evidence for a key role of phase and phase-amplitude relationships in motor goal encoding, and execution. These original findings extend previous invasive electrophysiological studies in humans that have investigated the correlates of motor intention and/or execution. For the large part, such studies were primarily based on the estimation of cortical power modulations in multiple frequency components of the LFP, including beta and gamma range power modulations (Leuthardt et al., 2004; Crone et al., 2006; Miller et al., 2007; Gunduz et al., 2016). Nevertheless, there is some evidence suggesting a critical role for low-frequency phase and amplitude information in mediating movement parameters (Hammer et al., 2016, 2013; Jerbi et al., 2011, 2007; Milekovic et al., 2012; Miller et al., 2012; Waldert et al., 2009, 2008; Kajihara et al., 2015; Liu et al., 2011). Using ECoG recordings in epilepsy patients, Hammer and colleagues (2013) directly addressed the role of phase information in decoding movement kinematics (i.e. position, velocity, and acceleration). By separately exploring kinematics decoding with spectral amplitudes and phase of the low frequency component (LFC), the authors came to the conclusion that the ECoG LFC phase was in fact much more informative than amplitude (Hammer et al., 2013).

In theory, it is conceivable that our single-trial decoding in the low frequency range (e.g. VLFC decoding) is driven at least in part by the presence of phase-locking across trials.

For instance, our decoding results may be related to the presence of a Bereitschaftspotential (BP), since the latter varies with movement states and parameters (Birbaumer et al., 1990; Shibasaki and Hallett, 2006). A consistent phase-locking across trials related to such slow cortical potentials may substantially contribute for instance to the high VLFC phase decoding we observed. A key question is whether this VLFC phase feature provides higher decoding than the envelope or the low-pass filtered raw signal in the same frequency range. To address this interesting question, we conducted additional decoding analyses where we directly compared decoding performance (across all available data) with the 3 following types of features (a) low-pass filtered [0.1–1.5 Hz] raw signal, (b) [0.1–1.5 Hz] phase (VLFC) and the (c) [0.1–1.5 Hz] envelope. The results (Fig. 7) suggest that the phase of the low-frequency signal contains more relevant information than its envelope in terms of decoding. When contrasted to the low-pass filtered signal, the phase provided either comparable or higher (cf. planning vs rest) motor state decoding. Note that these results were obtained in single trial classification (as is the case with all the rest of our analyses). These findings imply that single-trial low-frequency components (which contribute, when averaged, to generating motor-related potentials) provide significant motor state decoding performances. Our results (Fig. 7) indicate that this low-frequency decoding appears to be, on a trial-by-trial basis, primarily driven by the phase of the low-pass signal, rather than its envelope.

A recent study demonstrated that the LFC signal may be more adapted to speed decoding than to velocity decoding (Hammer et al., 2016). These findings are globally in line with reports of low frequency range coherence (< 4 Hz) between limb speed and the activity of the primary motor cortex during continuous movements (Jerbi et al., 2007). Moreover, movement direction classification has been achieved with significant success using the LFC component, both, with invasive and non-invasive brain recordings (Jerbi et al., 2011; Waldert et al., 2009, 2008).

Our observation of the efficacy of low frequency brain signals in motor decoding is consistent with a few animal studies that have revealed a prominent role for frequencies (< 5 Hz) LFP components in decoding motor movements via recordings in primary motor and parietal cortices (e.g. Mehring et al., 2004; Averbek et al., 2005; Rickert, 2005).

The results of the current study differ from the above reports in

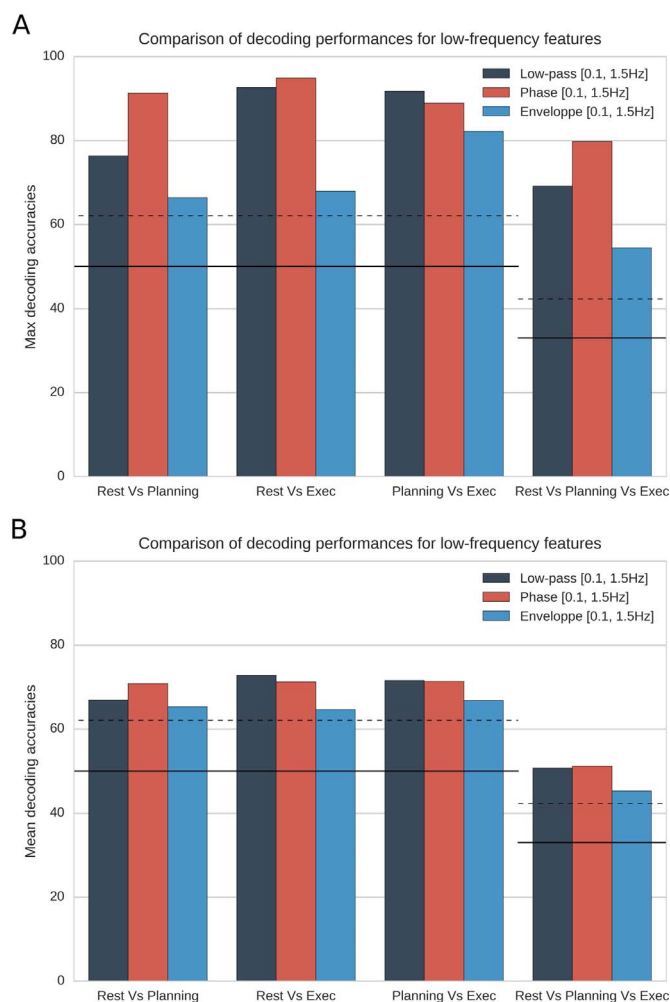


Fig. 7. Comparison of maximum decoding performance using 3 features in the same low frequency band (0.5–1.5 Hz): Low-pass filtered signal (dark blue), low-pass phase (red) and low-pass envelope (light blue). (A) Maximum decoding achieved with each feature type, and across the 4 classification problems. (B) Same as in (A) but here mean decoding across all statistically significant sites. In both panels, theoretical chance levels (50% or 33%) are depicted with continuous lines and the statistical thresholds ($p < 0.05$, corrected) are indicated by dashed lines. The low-frequency phase features provide higher classifications than the low-frequency envelope. The entire low-pass signal (dark blue) achieves decoding levels closer to those of the phase component. (For interpretation of the references to color in this figure legend, the reader is referred to the web version of this article.)

several ways. Firstly, while most studies typically focus on movement execution, the delayed-motor task used here allowed us to examine the role of phase information in the motor encoding and planning phase preceding actual movement execution. Secondly, beyond phase or amplitude, we performed a systematic exploration of PAC effects and found that it yielded significant modulations and motor state decoding. Thirdly, the intracerebral recordings of our subject pool provided a different spatial sampling compared to most previous electrocorticographic studies. In particular, the recording sites covered widely distributed brain areas beyond primary and secondary motor areas (such as parietal, prefrontal and insular cortices), and included some medial brain areas (e.g. dACC). Moreover, most of the previous investigations into the role of low frequencies (< 4 Hz) in movement decoding relied on the low-pass filtered brain signals. By contrast, we specifically focused on the phase at these low frequencies, but we also examined the difference with using the envelope or low-pass filtered signals (Fig. 7). Therefore, taken together, our exploration of intracranial recording during a delayed motor task confirms and extends the growing body of evidence for the role of phase and phase-related

measures in encoding motor processes, from intention to execution.

Invasive recordings in patients with motor disorders have been reported both with ECoG and passive recordings from deep brain stimulation (DBS) electrodes, in particular in the case of Parkinson's disease (McIntyre and Thakor, 2002; Litvak et al. 2011; Florin et al. 2013; Beudel et al. 2015; Rowland et al. 2015; Guridi and Alegre, 2016). For instance, the recent intracranial study by Rowland et al. (2015) bares some similarities with our study since it set out to explore beta and gamma power changes across rest, movement preparation and execution in Parkinson's patients. In particular, the authors used DBS recordings to monitor event-related synchronization and desynchronization associated with rigidity or akinesia in these patients. The study showed that compared to patients with essential tremor (who do not show rigidity or akinesia), Parkinson's patients had larger beta desynchronization in early motor preparation as well as enhanced cortical broadband gamma power during both rest and task. The authors interpret the findings as an indication that the dynamic profile of sensorimotor cortex oscillations in Parkinson's is in opposition with the anti-kinetic activity of the basal ganglia.

4.5. A key role for phase coding in goal-directed motor behavior

Currently, the overwhelming body of research on the oscillatory brain dynamics that mediate motor behavior continues to explore local activations in terms of amplitude modulations, while phase information is primarily used in the context of inter-regional connectivity assessments (da Silva, 2006; Lachaux et al., 1999; Le Van Quyen et al., 2001; Roach and Mathalon, 2008). Our findings support the view that phase carries critical information that is often overlooked, and can provide more task-specific information than spectral amplitude. Thus, one may wonder about the underlying physiological phenomenon that could explain the relevance of phase. One potential explanation is that phase modulations might be closely related to neuronal firing patterns. Evidence for this hypothesis has been found in non-human primates, for instance, in auditory and visual cortices (Ng et al., 2013; Montemurro et al., 2008). In the auditory cortex, stimulus selective firing patterns have been found to imprint on the phase, rather than the amplitude, of theta oscillations within both LFPs and EEG data (Ng et al. 2013). By applying a stimulus decoding technique to intracortical LFPs and single cell recordings in macaque auditory cortex, the authors found that the stimuli, which were successfully discriminated by firing rates, were also discriminated by phase patterns but not by oscillation amplitude. In visual cortex, information theoretical approaches have also shown that the combination of spikes and low frequency (1–4 Hz) LFP phase provide more information on visual stimuli than spikes alone (Latham and Lengyel, 2008; Montemurro et al., 2008). Similarly, the timing of action potentials relative to LFP theta phase in the hippocampus have been found to be more informative about position (i.e., higher precision) than what could be inferred from firing rate alone (Dragoi and Buzsáki, 2006; O'Keefe and Recce, 1993).

In the present study, the low-frequency phase decoding results could be theoretically explained by (and be consistent with) the hypothesis that the precise relationship between slow LFP phase and neuronal firing reported in other modalities (as discussed above), also operates in human motor brain areas during limb movement preparation and execution. This idea needs to be tested with microelectrode data allowing for simultaneous access to both LFP and neuronal firing in human participants. This was not possible with the SEEG data used for the purpose of this study. Furthermore, the significant modulations and decoding results reported here, using phase-amplitude coupling, could be suggestive of a specific mechanism by which phase, broadband gamma amplitude and neuronal firing are lined up in a precise fashion. Whittingstall and Logothetis (2009) observed such a phenomenon in macaque visual cortex, where multi-unit firing responses were found to be strongest only when increases in EEG gamma power occurred during a specific phase of the delta (2–4 Hz) wave. It is however

obvious that, the tempting speculation that this may also be at play in areas where we found significant PAC decoding, cannot be confirmed without simultaneous monitoring of neuronal firing.

While the notion of phase coding is not new *per se*, the presented results extend an emerging body of literature suggesting that phase coding may play a more important role in motor behavior than previously assumed. In particular, we found that phase-based motor state decoding (i) is widely distributed, extending beyond primary motor areas, (ii) occurs both during action planning and execution, and (iii) that phase-amplitude coupling could be an additional phase-based key feature involved in the neuronal coding of goal-directed behavior.

4.6. Limitations and open questions

The results of this study have a number of limitations. Our data, just like all previous intracranial EEG studies, have limited spatial sampling of the involved networks. The over 500 intracerebral sites used here provide only a partial spatial coverage of the brain, with a more dense coverage of right frontal than left frontal regions (Fig. 1A). Additionally, a reliable comparison between neural responses contra and ipsilateral to the moving hand was not possible because 4 patients out of 6 had uni-lateral implantations, and even for those with bilateral implantation, the electrodes were not located in exact homologous brain areas in both hemispheres. This is a typical limitation of invasive human data. Clearly, investigating the lateralization of amplitude, phase and PAC phenomena reported here, would greatly benefit from further investigations with full head coverage using MEG or EEG and similar delayed-motor paradigms. This said, patients were selected primarily based on whether they had electrodes implanted in frontal, prefrontal or parietal areas, thus providing a reasonable coverage of the targeted networks. Moreover, as in all previous human invasive recordings, participants suffered from drug-resistant epilepsy, which could limit the generalizability of the findings to healthy subjects. To address this in the best possible way, our standard procedure (e.g. Jerbi et al., 2009) is to exclude electrodes that display pathological activity (such as epileptic spikes), and to focus on task-related changes and multi-trial analyses, thereby reducing the impact of neuronal activations that are spurious or unrelated to the task. Therefore, our findings could benefit from future replication using non-invasive recordings in healthy controls.

Note that all the decoding throughout this study was performed on single-features in single-trial mode, individually in each subject. We did not use multi-feature classifications, and did not pool all participants in the decoder. The nature of the individualized SEEG implantation precludes the possibility to reliably combine data from multiple subjects into the same cross-validation decoding framework. We chose to provide an overview of the single-feature findings across BAs (mean and max significant decoding accuracies, Fig. 6) as a pragmatic way to pool the multi-subject results. Of course, the decoding accuracies would have likely been even higher had we chosen to run multi-feature classification at least within individual subjects. Yet, our aim was not to achieve the highest decoding rate, rather to use the decoding approach to unravel and compare the distinct contribution of each feature individually to motor planning and execution processes.

Furthermore, it is important to acknowledge that our task design did not allow for a fine-grained disambiguation of the various, distinct, processes that are expected to take place during the delay period. Clearly, the delay period encompasses a wide range of processes, such as stimulus encoding, visuomotor transformations, motor imagery, action selection, motor preparation, as well as working memory and maintenance processes. To limit any bias towards visual stimulus encoding when analyzing the planning/intention period, we deliberately centered our phase and amplitude analyses on 500 ms after target onset. In future investigations, this limitation should be addressed with a specific experimental design aimed at disentangling various motor related processes in the delay period.

In addition, the Go cue is likely to be immediately followed both by preparatory and execution signals. Thus, a more detailed analysis of motor execution would have been possible if we were able to align the data to movement onset rather than the Go cue. Unfortunately, for technical reasons movement onset was not available. To limit the impact of this limitation, we deliberately considered a window in the execution phase between 500 ms and 1000 ms after the Go Cue, and thus ignored the 500 ms post-Go period where most of the preparation is expected to take place. More importantly, because we relied on a decoding approach to disentangle execution from preparation, we hypothesized that processes (or feature modulations) common to both conditions would not allow for significant decoding, and thus by definition, features with high decoding should reflect differences between the two states.

Moreover, the physiological interpretations made in the current study also bare their share of limitations. The way the explored features (amplitude, phase and PAC) explicitly relate to the notion of information processing in the human brain is still poorly understood. Rather than identifying the precise functional relevance of each feature, our results emphasized their task-specific modulations and their ability to successfully predict the state of the system in single-trial data (i.e. Rest, motor Planning or motor Execution).

Despite the above limitations, we feel that access to intracerebral depth EEG recordings in human subjects, provides privileged insight into the neural dynamics mediating human cognition, with superior spatial, temporal and spectral precision. In the long run, this type of data can help bridge the gap between neuroimaging studies and electrophysiological recordings in non-human primates.

5. Conclusion

The findings of this study provide novel experimental evidence for the role of oscillatory phase and amplitude properties in motor planning and execution. In particular, the evidence for phase and PAC-based coding are a compelling support for the key role of phase in encoding motor representations and mediating movement execution across widely distributed brain areas. We are confident that these results will pave the way for a better understanding of, and novel hypotheses about, the roles of phase, amplitude, and the coordination between the two, in goal-directed motor behavior in humans.

Conflict of interest

The authors declare that there is no conflict of interests regarding the publication of this paper.

Acknowledgments

Etienne Combrisson was supported in part by a Ph.D. Scholarship awarded by the Ecole Doctorale Inter-Disciplinaire Sciences-Santé (EDISS), Lyon, France, and by Ph.D. funding from the Natural Sciences and Engineering Research Council of Canada (NSERC). This work was partly performed within the framework of the LABEX CORTEX (ANR-11-LABX-0042) of Université de Lyon, within the program ANR-11-IDEX-0007, and by the ANR (project FORCE, ANR-13-TECS-0013-01), SEMAINE, the Human Brain Project (Human intracerebral database, Grant number 604102) to J.-P. Lachaux; We acknowledge support from the Brazilian Ministry of Education (CAPES grant 1719-04-1), the Fondation pour la Recherche Médicale (FRM, France) and the Fulbright Commission to J.L.P. Soto, and funding from the Canada Research Chairs program and a Discovery Grant (RGPIN-2015-04854) awarded by the Natural Sciences and Engineering Research Council of Canada to K.J. The authors are grateful for the collaboration of the patients and clinical staff at the Epilepsy Department of the Grenoble University Hospital.

Appendix A. Supplementary material

Supplementary data associated with this article can be found in the online version at <http://dx.doi.org/10.1016/j.neuroimage.2016.11.042>.

References

- Ariani, G., Wurm, M.F., Lingnau, A., 2015. Decoding internally and externally driven movement plans. *J. Neurosci. Off. J. Soc. Neurosci.* 35, 14160–14171. <http://dx.doi.org/10.1523/JNEUROSCI.0596-15.2015>.
- Aru, J., Aru, J., Priesemann, V., Wibral, M., Lana, L., Pipa, G., Singer, W., Vicente, R., 2015. Untangling cross-frequency coupling in neuroscience. *Curr. Opin. Neurobiol. SI: Brain Rhythm. Dyn. Coord.* 31, 51–61. <http://dx.doi.org/10.1016/j.conb.2014.08.002>.
- Averbeck, B.B., Chafee, M.V., Crowe, D.A., Georgopoulos, A.P., 2005. Parietal representation of hand velocity in a copy task. *J. Neurophysiol.* 93, 508–518.
- Babiloni, C., Del Percio, C., Vecchio, F., Sebastiano, F., Di Gennaro, G., Quarato, P.P., Morace, R., Pavone, L., Soricelli, A., Noce, G., Esposito, V., Rossini, P.M., Gallese, V., Mirabella, G., 2016. Alpha, beta and gamma electrocorticographic rhythms in somatosensory, motor, premotor and prefrontal cortical areas differ in movement execution and observation in humans. *Clin. Neurophysiol. Off. J. Int. Fed. Clin. Neurophysiol.* 127, 641–654. <http://dx.doi.org/10.1016/j.clinph.2015.04.068>.
- Babiloni, C., Babiloni, F., Carducci, F., Cincotti, F., Rosciarelli, F., Arendt-Nielsen, L., Chen, A.C.N., Rossini, P.M., 2002. Human brain oscillatory activity phase-locked to painful electrical stimulations: a multi-channel EEG study. *Hum. Brain Mapp.* 15, 112–123. <http://dx.doi.org/10.1002/hbm.10013>.
- Bahramisharif, A., van Gerven, M.A.J., Aarnoutse, E.J., Mercier, M.R., Schwartz, T.H., Foxe, J.J., Ramsey, N.F., Jensen, O., 2013. Propagating neocortical gamma bursts are coordinated by traveling alpha waves. *J. Neurosci.* 33, 18849–18854. <http://dx.doi.org/10.1523/JNEUROSCI.2455-13.2013>.
- Ball, T., Schreiber, A., Feige, B., Wagner, M., Lücking, C.H., Kristeva-Feige, R., 1999. The role of higher-order motor areas in voluntary movement as revealed by high-resolution EEG and fMRI. *Neuroimage* 10, 682–694.
- Ball, T., Demandt, E., Mutschler, I., Neitzel, E., Mehring, C., Vogt, K., Aertsen, A., Schulze-Bonhage, A., 2008. Movement related activity in the high gamma range of the human EEG. *Neuroimage* 41, 302–310.
- Bastin, J., Deman, P., David, O., Gueguen, M., Benis, D., Minotti, L., Hoffman, D., Combrisson, E., Kujala, J., Perrone-Bertolotti, M., Kahane, P., Lachaux, J.-P., Jerbi, K., 2016. Direct recordings from human anterior insula reveal its leading role within the error-monitoring network. *Cereb. Cortex Behav.* 352. <http://dx.doi.org/10.1093/cercor/bhv352>.
- Berens, P., et al., 2009. CircStat a MATLAB toolbox for circular statistics. *J. Stat. Softw.* 31, 1–21.
- Beudel, M., Little, S., Poghosyan, A., Ashkan, K., Foltynie, T., Limousin, P., Zrinzo, L., Hariz, M., Bogdanovic, M., Cheeran, B., others, 2015. Tremor reduction by deep brain stimulation is associated with gamma power suppression in Parkinson's disease. *Neuromodul.: Technol. Neural Interface* 18, 349–354.
- Birbaumer, N., Elbert, T., Canavan, A.G., Rockstroh, B., 1990. Slow potentials of the cerebral cortex and behavior. *Physiol. Rev.* 70, 1–41.
- Brovelli, A., Lachaux, J.-P., Kahane, P., Boussaoud, D., 2005. High gamma frequency oscillatory activity dissociates attention from intention in the human premotor cortex. *Neuroimage* 28, 154–164. <http://dx.doi.org/10.1016/j.neuroimage.2005.05.045>.
- Bundy, D.T., Pahwa, M., Szrama, N., Leuthardt, E.C., 2016. Decoding three-dimensional reaching movements using electrocorticographic signals in humans. *J. Neural Eng.* 13, 026021. <http://dx.doi.org/10.1088/1741-2560/13/2/026021>.
- Canolty, R.T., 2006. High gamma power is phase-locked to theta. *Science* 1128115, 313.
- Canolty, R.T., Knight, R.T., 2010. The functional role of cross-frequency coupling. *Trends Cogn. Sci.* 14 (11), 506–515. <http://dx.doi.org/10.1016/j.tics.2010.09.001>.
- Caspers, S., Eickhoff, S.B., Geyer, S., Scheperjans, F., Mohlberg, H., Zilles, K., Amunts, K., 2008. The human inferior parietal lobe in stereotaxic space. *Brain Struct. Funct.* 212, 481–495. <http://dx.doi.org/10.1007/s00429-008-0195-z>.
- Cheyne, D.O., Ferrari, P., Cheyne, J.A., 2012. Intended actions and unexpected outcomes: automatic and controlled processing in a rapid motor task. *Front. Hum. Neurosci.* 6, 237. <http://dx.doi.org/10.3389/fnhum.2012.00237>.
- Cheyne, D., Bells, S., Ferrari, P., Gaetz, W., Bostan, A.C., 2008. Self-paced movements induce high-frequency gamma oscillations in primary motor cortex. *Neuroimage* 42, 332–342. <http://dx.doi.org/10.1016/j.neuroimage.2008.04.178>.
- Cohen, M.X., Elger, C.E., Fell, J., 2008. Oscillatory activity and phase–amplitude coupling in the human medial frontal cortex during decision making. *J. Cogn. Neurosci.* 21, 390–402.
- Combrisson, E., Jerbi, K., 2015. Exceeding chance level by chance: the caveat of theoretical chance levels in brain signal classification and statistical assessment of decoding accuracy. *J. Neurosci. Methods* 250, 126–136. <http://dx.doi.org/10.1016/j.jneumeth.2015.01.010>.
- Crone, N., 1998. Functional mapping of human sensorimotor cortex with electrocorticographic spectral analysis I. Alpha and beta event-related desynchronization. *Brain* 121, 2271–2299. <http://dx.doi.org/10.1093/brain/121.12.2271>.
- Crone, N.E., Miglioretti, D.L., Gordon, B., Lesser, R.P., 1998. Functional mapping of human sensorimotor cortex with electrocorticographic spectral analysis II. Event-related synchronization in the gamma band. *Brain*, 2301–2315.

- Crone, N.E., Sinai, A., Korzeniewska, A., 2006. High-frequency gamma oscillations and human brain mapping with electrocorticography. In: *Progress in Brain Research*. Elsevier, pp. 275–295.
- da Silva, F.H.L., 2006. Event-related neural activities: what about phase? *Prog. Brain Res.* 159, 3–17.
- Delorme, A., Makeig, S., 2004. EEGLAB: an open source toolbox for analysis of single-trial EEG dynamics including independent component analysis. *J. Neurosci. Methods* 134, 9–21.
- Desmurget, M., Sirigu, A., 2009. A parietal-premotor network for movement intention and motor awareness. *Trends Cogn. Sci.* 13, 411–419. <http://dx.doi.org/10.1016/j.tics.2009.08.001>.
- Dragoi, G., Buzsáki, G., 2006. Temporal encoding of place sequences by hippocampal cell assemblies. *Neuron* 50, 145–157. <http://dx.doi.org/10.1016/j.neuron.2006.02.023>.
- Drewes, J., VanRullen, R., 2011. This is the rhythm of your eyes: the phase of ongoing electroencephalogram oscillations modulates saccadic reaction time. *J. Neurosci.* 31, 4698–4708. <http://dx.doi.org/10.1523/JNEUROSCI.4795-10.2011>.
- Dugue, L., Marque, P., VanRullen, R., 2011. The phase of ongoing oscillations mediates the causal relation between brain excitation and visual perception. *J. Neurosci.* 31, 11889–11893. <http://dx.doi.org/10.1523/JNEUROSCI.1161-11.2011>.
- Florin, E., Erasmi, R., Reck, C., Maarouf, M., Schnitzler, A., Fink, G., Timmermann, L., 2013. Does increased gamma activity in patients suffering from Parkinson's disease counteract the movement inhibiting beta activity? *Neuroscience* 237, 42–50.
- Foster, B.L., Parvizi, J., 2012. Resting oscillations and cross-frequency coupling in the human posteromedial cortex. *Neuroimage* 60, 384–391. <http://dx.doi.org/10.1016/j.neuroimage.2011.12.019>.
- Gallivan, J.P., McLean, D.A., Flanagan, J.R., Culham, J.C., 2013. Where one hand meets the other: limb-specific and action-dependent movement plans decoded from preparatory signals in single human frontoparietal brain areas. *J. Neurosci.* 33, 1991–2008.
- Golland, P., Fischl, B., 2003. Permutation tests for classification: towards statistical significance in image-based studies. In: *Proceedings of the 18th Conference of Information Processing in Medical Imaging*, pp. 330–341.
- Guillot, A., Di Rienzo, F., MacIntyre, T., Moran, A., Collet, C., 2012. Imagining is not doing but involves specific motor commands: a review of experimental data related to motor inhibition. *Front. Hum. Neurosci.* 6, 247.
- Gunduz, A., Brunner, P., Sharma, M., Leuthardt, E.C., Ritaccio, A.L., Pesaran, B., Schalk, G., 2016. Differential roles of high gamma and local motor potentials for movement preparation and execution. *Brain-Computer Interfaces* 3, 88–102. <http://dx.doi.org/10.1080/2326263X.2016.1179087>.
- Guridi, J., Alegre, M., 2016. Oscillatory activity in the basal ganglia and deep brain stimulation. *Mov. Disord.*
- Hamamé, C.M., Vidal, J.R., Perrone-Bertolotti, M., Ossandón, T., Jerbi, K., Kahane, P., Bertrand, O., Lachaux, J.-P., 2014. Functional selectivity in the human occipitotemporal cortex during natural vision: evidence from combined intracranial EEG and eye-tracking. *Neuroimage* 95, 276–286.
- Hammer, J., Fischer, J., Ruescher, J., Schulze-Bonhage, A., Aertsen, A., Ball, T., 2013. The role of ECoG magnitude and phase in decoding position, velocity, and acceleration during continuous motor behavior. *Front. Neurosci.*, 7. <http://dx.doi.org/10.3389/fnins.2013.00200>.
- Hammer, J., Pistohl, T., Fischer, J., Kršek, P., Tomášek, M., Marušić, P., Schulze-Bonhage, A., Aertsen, A., Ball, T., 2016. Predominance of movement speed over direction in neuronal population signals of motor cortex: intracranial EEG data and a simple explanatory model. *Cereb. Cortex* 26, 2863–2881. <http://dx.doi.org/10.1093/cercor/bhw033>.
- Hanakawa, T., Dimyan, M.A., Hallett, M., 2008. Motor planning, imagery, and execution in the distributed motor network: a time-course study with functional MRI. *Cereb. Cortex* 18, 2775–2788. <http://dx.doi.org/10.1093/cercor/bhn036>.
- Hempton, C. de, Ryapolova-Webb, E.S., Air, E.L., Garcia, P.A., Miller, K.J., Ojemann, J.G., Ostrem, J.L., Galifianakis, N.B., Starr, P.A., 2013. Exaggerated phase-amplitude coupling in the primary motor cortex in Parkinson disease. *Proc. Natl. Acad. Sci. USA*. <http://dx.doi.org/10.1073/pnas.1214546110>.
- Hyafil, A., Giraud, A.-L., Fontolan, L., Gutkin, B., 2015. Neural cross-frequency coupling: connecting architectures, mechanisms, and functions. *Trends Neurosci.* 38, 725–740. <http://dx.doi.org/10.1016/j.tics.2015.09.001>.
- Jahanshahi, M., Jenkins, I.H., Brown, R.G., Marsden, C.D., Passingham, R.E., Brooks, D.J., 1995. Self-initiated versus externally triggered movements. I. An investigation using measurement of regional cerebral blood flow with PET and movement-related potentials in normal and Parkinson's disease subjects. *Brain J. Neurol.* 118 (Pt 4), 913–933.
- Jenkinson, N., Kühn, A.A., Brown, P., 2013. Gamma oscillations in the human basal ganglia. *Exp. Neurol.* 245, 72–76. <http://dx.doi.org/10.1016/j.expneurol.2012.07.005>.
- Jeanerod, M., 1994. The representing brain: neural correlates of motor intention and imagery. *Behav. Brain Sci.* 17, 187–202.
- Jensen, O., Colgin, L.L., 2007. Cross-frequency coupling between neuronal oscillations. *Trends Cogn. Sci.* 11, 267–269. <http://dx.doi.org/10.1016/j.tics.2007.05.003>.
- Jensen, O., Gips, B., Bergmann, T.O., Bonnefond, M., 2014. Temporal coding organized by coupled alpha and gamma oscillations prioritize visual processing. *Trends Neurosci.* 37, 357–369. <http://dx.doi.org/10.1016/j.tics.2014.04.001>.
- Jerbi, K., Lachaux, J.-P., Karim, N., Pantazis, D., Leahy, R.M., Garnero, L., Baillet, S., others, 2007. Coherent neural representation of hand speed in humans revealed by MEG imaging. *Proc. Natl. Acad. Sci.* 104, 7676–7681.
- Jerbi, K., Ossandón, T., Hamamé, C.M., Senova, S., Dalal, S.S., Jung, J., Minotti, L., Bertrand, O., Berthoz, A., Kahane, P., Lachaux, J.-P., 2009. Task-related gamma-band dynamics from an intracerebral perspective: review and implications for surface EEG and MEG. *Hum. Brain Mapp.* 30, 1758–1771. <http://dx.doi.org/10.1002/hbm.20750>.
- Jerbi, K., Vidal, J.R., Mattout, J., Maby, E., Lecaigard, F., Ossandón, T., Hamamé, C.M., Dalal, S.S., Bouet, R., Lachaux, J.-P., Leahy, R.M., Baillet, S., Garnero, L., Delpuech, C., Bertrand, O., 2011. Inferring hand movement kinematics from MEG, EEG and intracranial EEG: from brain-machine interfaces to motor rehabilitation. *IRBM* 32, 8–18. <http://dx.doi.org/10.1016/j.irbm.2010.12.004>.
- Jerbi, K., Vidal, J.R., Ossandón, T., Dalal, S.S., Jung, J., Hoffmann, D., Minotti, L., Bertrand, O., Kahane, P., Lachaux, J.-P., 2010. Exploring the electrophysiological correlates of the default-mode network with intracerebral EEG. *Front. Syst. Neurosci.* 4, 27. <http://dx.doi.org/10.3389/fnys.2010.00027>.
- Jurkiewicz, M.T., Gaetz, W.C., Bostan, A.C., Cheyne, D., 2006. Post-movement beta rebound is generated in motor cortex: evidence from neuromagnetic recordings. *Neuroimage* 32, 1281–1289. <http://dx.doi.org/10.1016/j.neuroimage.2006.06.005>.
- Kahane, P., Landré, E., Minotti, L., Francione, S., Ryvlin, P., 2006. The Bancaud and Talairach view on the epileptogenic zone: a working hypothesis. *Epileptic Disord. Int. Epilepsy J. Videotape* 8, S16–S26.
- Kajihara, T., Anwar, M.N., Kawasaki, M., Mizuno, Y., Nakazawa, K., Kitajo, K., 2015. Neural dynamics in motor preparation: from phase-mediated global computation to amplitude-mediated local computation. *Neuroimage* 118, 445–455. <http://dx.doi.org/10.1016/j.neuroimage.2015.05.032>.
- Kalaska, J.F., 2009. From intention to action: motor cortex and the control of reaching movements. In: Sternad, D. (Ed.), *Progress in Motor Control*. Springer US, Boston, MA, 139–178.
- Klimesch, W., Freunberger, R., Sauseng, P., Gruber, W., 2008. A short review of slow phase synchronization and memory: evidence for control processes in different memory systems? *Brain Res. Brain Oscil. Cogn. Cogn. Disord.* 1235, 31–44. <http://dx.doi.org/10.1016/j.brainres.2008.06.049>.
- Klimesch, W., Sauseng, P., Hanslmayr, S., 2007. EEG alpha oscillations: the inhibition-timing hypothesis. *Brain Res. Rev.* 53, 63–88. <http://dx.doi.org/10.1016/j.brainresrev.2006.06.003>.
- Kramer, M.A., Tort, A.B.L., Kopell, N.J., 2008. Sharp edge artifacts and spurious coupling in EEG frequency comodulation measures. *J. Neurosci. Methods* 170, 352–357. <http://dx.doi.org/10.1016/j.jneumeth.2008.01.020>.
- Lachaux, J.-P., Rodriguez, E., Martinerie, J., Varela, F.J., et al., 1999. Measuring phase synchrony in brain signals. *Hum. Brain Mapp.* 8, 194–208.
- Lachaux, J.P., Rudrauf, D., Kahane, P., 2003. Intracranial EEG and human brain mapping. *J. Physiol. Paris* 97, 613–628. <http://dx.doi.org/10.1016/j.jphysparis.2004.01.018>.
- Lacourse, M.G., Orr, E.L.R., Cramer, S.C., Cohen, M.J., 2005. Brain activation during execution and motor imagery of novel and skilled sequential hand movements. *Neuroimage* 27, 505–519. <http://dx.doi.org/10.1016/j.neuroimage.2005.04.025>.
- Lakatos, P., 2005. An oscillatory hierarchy controlling neuronal excitability and stimulus processing in the auditory cortex. *J. Neurophysiol.* 94, 1904–1911. <http://dx.doi.org/10.1152/jn.00263.2005>.
- Latham, P.E., Lengyel, M., 2008. Phase coding: spikes get a boost from local fields. *Curr. Biol.* 18, R349–R351. <http://dx.doi.org/10.1016/j.cub.2008.02.062>.
- Lau, H.C., 2004. Attention to intention. *Science* 303, 1208–1210. <http://dx.doi.org/10.1126/science.1090973>.
- Le Van Quyen, M., Foucher, J., Lachaux, J.-P., Rodriguez, E., Lutz, A., Martinerie, J., Varela, F.J., 2001. Comparison of Hilbert transform and wavelet methods for the analysis of neuronal synchrony. *J. Neurosci. Methods* 111, 83–98.
- Lee, J., Jeong, J., 2013. Correlation of risk-taking propensity with cross-frequency phase-amplitude coupling in the resting EEG. *Clin. Neurophysiol.* <http://dx.doi.org/10.1016/j.clinph.2013.05.007>.
- Lemm, S., Blankertz, B., Dickhaus, T., Müller, K.-R., 2011. Introduction to machine learning for brain imaging. *Neuroimage* 56, 387–399. <http://dx.doi.org/10.1016/j.neuroimage.2010.11.004>.
- Leuthardt, E.C., Schalk, G., Wolpaw, J.R., Ojemann, J.G., Moran, D.W., 2004. A brain-computer interface using electrocorticographic signals in humans. *J. Neural Eng.* 1, 63. <http://dx.doi.org/10.1088/1741-2560/1/2/001>.
- Litvak, V., Jha, A., Eusebio, A., Oostenveld, R., Foltynie, T., Limousin, P., Zrinzo, L., Hariz, M.I., Friston, K., Brown, P., 2011. Resting oscillatory cortico-subthalamic connectivity in patients with Parkinson's disease. *Brain* 134, 359–374. <http://dx.doi.org/10.1093/brain/awq332>.
- Liu, J., Perdoni, C., He, B., 2011. Hand movement decoding by phase-locking low frequency EEG signals. In: *Proceedings of the Annual International Conference IEEE Engineering in Medicine and Biology Society*. doi:10.1109/IEMBS.2011.6091564. pp. 6335–6338.
- Maris, E., van Vugt, M., Kahana, M., 2011. Spatially distributed patterns of oscillatory coupling between high-frequency amplitudes and low-frequency phases in human iEEG. *Neuroimage* 54, 836–850.
- Mattingley, J.B., Husain, M., Rorden, C., Kennard, C., Driver, J., 1998. Motor role of human inferior parietal lobe revealed in unilateral neglect patients. *Nature* 392, 179–182. <http://dx.doi.org/10.1038/32413>.
- McIntyre, C.C., Thakor, N.V., 2002. Uncovering the mechanisms of deep brain stimulation for Parkinson's disease through functional imaging, neural recording, and neural modeling. *Crit. Rev. Biomed. Eng.*, 30.
- Mehring, C., Nawrot, M.P., de Oliveira, S.C., Vaadia, E., Schulze-Bonhage, A., Aertsen, A., Ball, T., 2004. Comparing information about arm movement direction in single channels of local and epicortical field potentials from monkey and human motor cortex. *J. Physiol. Paris* 98, 498–506. <http://dx.doi.org/10.1016/j.jphysparis.2005.09.016>.
- Meyers, E., Kreiman, G., 2012. Tutorial on pattern classification in cell recording. *Vis. Popul. Codes*, 517–538.
- Milekovic, T., Fischer, J., Pistohl, T., Ruescher, J., Schulze-Bonhage, A., Aertsen, A., Rickert, J., Ball, T., Mehring, C., 2012. An online brain-machine interface using

- decoding of movement direction from the human electrocorticogram. *J. Neural Eng.* 9, 046003. <http://dx.doi.org/10.1088/1741-2560/9/4/046003>.
- Miller, K.J., denNijs, M., Shenoy, P., Miller, J.W., Rao, R.P.N., Ojemann, J.G., 2007. Real-time functional brain mapping using electrocorticography. *Neuroimage* 37, 504–507. <http://dx.doi.org/10.1016/j.neuroimage.2007.05.029>.
- Miller, K.J., Schalk, G., Fetz, E.E., den Nijs, M., Ojemann, J.G., Rao, R.P., 2010. Cortical activity during motor execution, motor imagery, and imagery-based online feedback. *Proc. Natl. Acad. Sci.* 107, 4430–4435.
- Miller, K.J., Hermes, D., Honey, C.J., Hebb, A.O., Ramsey, N.F., Knight, R.T., Ojemann, J.G., Fetz, E.E., 2012. Human motor cortical activity is selectively phase-entrained on underlying rhythms. *PLoS Comput. Biol.* 8, e1002655. <http://dx.doi.org/10.1371/journal.pcbi.1002655>.
- Montemurro, M.A., Rasch, M.J., Murayama, Y., Logothetis, N.K., Panzeri, S., 2008. Phase-of-firing coding of natural visual stimuli in primary visual cortex. *Curr. Biol.* 18, 375–380. <http://dx.doi.org/10.1016/j.cub.2008.02.023>.
- Muthukumaraswamy, S.D., 2010. Functional properties of human primary motor cortex gamma oscillations. *J. Neurophysiol.* 104, 2873–2885.
- Muthukumaraswamy, S.D., 2011. Temporal dynamics of primary motor cortex gamma oscillation amplitude and piper corticomuscular coherence changes during motor control. *Exp. Brain Res.* 212, 623–633.
- Nakhnikian, A., Ito, S., Dwiell, L.L., Grasse, L.M., Rebec, G.V., Lauridsen, L.N., Beggs, J.M., 2016. A novel cross-frequency coupling detection method using the generalized morse wavelets. *J. Neurosci. Methods* 269, 61–73. <http://dx.doi.org/10.1016/j.jneumeth.2016.04.019>.
- Newman, E.L., Gillet, S.N., Climer, J.R., Hasselmo, M.E., 2013. Cholinergic blockade reduces theta-gamma phase amplitude coupling and speed modulation of theta frequency consistent with behavioral effects on encoding. *J. Neurosci.* 33, 19635–19646. <http://dx.doi.org/10.1523/JNEUROSCI.2586-13.2013>.
- Ng, B.S.W., Logothetis, N.K., Kayser, C., 2013. EEG phase patterns reflect the selectivity of neural firing. *Cereb. Cortex* 23, 389–398. <http://dx.doi.org/10.1093/cercor/bhs031>.
- O'Keefe, J., Recce, M.L., 1993. Phase relationship between hippocampal place units and the EEG theta rhythm. *Hippocampus* 3, 317–330.
- Ojala, M., Garriga, G.C., 2010. Permutation tests for studying classifier performance. *J. Mach. Learn. Res.* 11, 1833–1863.
- Ossandon, T., Jerbi, K., Vidal, J.R., Bayle, D.J., Henaff, M.-A., Jung, J., Minotti, L., Bertrand, O., Kahane, P., Lachaux, J.-P., 2011. Transient suppression of broadband gamma power in the default-mode network is correlated with task complexity and subject performance. *J. Neurosci.* 31, 14521–14530. <http://dx.doi.org/10.1523/JNEUROSCI.2483-11.2011>.
- Ossandon, T., Vidal, J.R., Ciumas, C., Jerbi, K., Hamame, C.M., Dalal, S.S., Bertrand, O., Minotti, L., Kahane, P., Lachaux, J.-P., 2012. Efficient “pop-out” visual search elicits sustained broadband gamma activity in the dorsal attention network. *J. Neurosci.* 32, 3414–3421. <http://dx.doi.org/10.1523/JNEUROSCI.6048-11.2012>.
- Ozkurt, T.E., 2012. Statistically reliable and fast direct estimation of phase-amplitude cross-frequency coupling. *Biomed. Eng. IEEE Trans.* 59, 1943–1950.
- Özkurt, T.E., Schnitzler, A., 2011. A critical note on the definition of phase–amplitude cross-frequency coupling. *J. Neurosci. Methods* 201, 438–443. <http://dx.doi.org/10.1016/j.jneumeth.2011.08.014>.
- Palva, S., Palva, J.M., 2007. New vistas for α -frequency band oscillations. *Trends Neurosci.* 30, 150–158. <http://dx.doi.org/10.1016/j.tins.2007.02.001>.
- Paus, T., 2001. Primate anterior cingulate cortex: where motor control, drive and cognition interface. *Nat. Rev. Neurosci.* 2, 417–424. <http://dx.doi.org/10.1038/35077500>.
- Perrone-Bertolotti, M., Kujala, J., Vidal, J.R., Hamame, C.M., Ossandon, T., Bertrand, O., Minotti, L., Kahane, P., Jerbi, K., Lachaux, J.-P., 2012. How silent is silent reading? Intracerebral evidence for top-down activation of temporal voice areas during reading. *J. Neurosci.* 32, 17554–17562.
- Pfurtscheller, G., Lopes da Silva, F.H., 1999. Event-related EEG/MEG synchronization and desynchronization: basic principles. *Clin. Neurophysiol.* 110, 1842–1857.
- Pfurtscheller, G., Graimann, B., Huggins, J.E., Levine, S.P., Schuh, L.A., 2003. Spatiotemporal patterns of beta desynchronization and gamma synchronization in corticographic data during self-paced movement. *Clin. Neurophysiol.* 114, 1226–1236. [http://dx.doi.org/10.1016/S1388-2457\(03\)00067-1](http://dx.doi.org/10.1016/S1388-2457(03)00067-1).
- Pittman-Polletta, B., Hsieh, W.-H., Kaur, S., Lo, M.-T., Hu, K., 2014. Detecting phase-amplitude coupling with high frequency resolution using adaptive decompositions. *J. Neurosci. Methods* 226, 15–32. <http://dx.doi.org/10.1016/j.jneumeth.2014.01.006>.
- Ray, S., Maunsell, J.H., 2011. Different origins of gamma rhythm and high-gamma activity in macaque visual cortex. *PLoS Biol.* 9, e1000610.
- Rektor, I., Sochůrková, D., Bocková, M., 2006. Intracerebral ERD/ERS in voluntary movement and in cognitive visuomotor task. *Prog. Brain Res.* 159, 311–330. [http://dx.doi.org/10.1016/S0079-6123\(06\)59021-1](http://dx.doi.org/10.1016/S0079-6123(06)59021-1).
- Rickert, J., 2005. Encoding of movement direction in different frequency ranges of motor cortical local field potentials. *J. Neurosci.* 25, 8815–8824. <http://dx.doi.org/10.1523/JNEUROSCI.0816-05.2005>.
- Roach, B.J., Mathalon, D.H., 2008. Event-related EEG time-frequency analysis: an overview of measures and an analysis of early gamma band phase locking in schizophrenia. *Schizophr. Bull.* 34, 907–926.
- Rowland, N.C., De Hemptinne, C., Swann, N.C., Qasim, S., Miciocinovic, S., Ostrem, J.L., Knight, R.T., Starr, P.A., 2015. Task-related activity in sensorimotor cortex in Parkinson's disease and essential tremor: changes in beta and gamma bands. *Front. Hum. Neurosci.* 9. <http://dx.doi.org/10.3389/fnhum.2015.00512>.
- Rushworth, M.F., Krams, M., Passingham, R.E., 2001. The attentional role of the left parietal cortex: the distinct lateralization and localization of motor attention in the human brain. *J. Cogn. Neurosci.* 13, 698–710. <http://dx.doi.org/10.1162/089989201750363244>.
- Saleh, M., Reimer, J., Penn, R., Ojakangas, C.L., Hatsopoulos, N.G., 2010. Fast and slow oscillations in human primary motor cortex predict oncoming behaviorally relevant cues. *Neuron* 65, 461–471. <http://dx.doi.org/10.1016/j.neuron.2010.02.001>.
- Sauseng, P., Klimesch, W., 2008. What does phase information of oscillatory brain activity tell us about cognitive processes? *Neurosci. Biobehav. Rev.* 32, 1001–1013. <http://dx.doi.org/10.1016/j.neubiorev.2008.03.014>.
- Schnitzler, A., Gross, J., 2005. Normal and pathological oscillatory communication in the brain. *Nat. Rev. Neurosci.* 6, 285–296. <http://dx.doi.org/10.1038/nrn1650>.
- Schwartz, A.B., 2016. Movement: how the brain communicates with the world. *Cell* 164, 1122–1135. <http://dx.doi.org/10.1016/j.cell.2016.02.038>.
- Sherman, M.T., Kanai, R., Seth, A.K., VanRullen, R., 2016. Rhythmic influence of top-down perceptual priors in the phase of prestimulus occipital alpha oscillations. *J. Cogn. Neurosci.*
- Shibasaki, H., Hallett, M., 2006. What is the Bereitschaftspotential? *Clin. Neurophysiol.* 117, 2341–2356. <http://dx.doi.org/10.1016/j.clinph.2006.04.025>.
- Snyder, L.H., Batista, A.P., Andersen, R.A., 1997. Coding of intention in the posterior parietal cortex. *Nature* 386, 167–170. <http://dx.doi.org/10.1038/386167a0>.
- Soto, J.L., Jerbi, K., 2012. Investigation of cross-frequency phase-amplitude coupling in visuomotor networks using magnetoencephalography. In: Proceedings of the Engineering in Medicine and Biology Society (EMBC), Annual International Conference of the IEEE, pp. 1550–1553.
- Staresina, B.P., Bergmann, T.O., Bonnefond, M., van der Meij, R., Jensen, O., Deuker, L., Elger, C.E., Axmacher, N., Fell, J., 2015. Hierarchical nesting of slow oscillations, spindles and ripples in the human hippocampus during sleep. *Nat. Neurosci.*
- Stephan, K.M., Fink, G.R., Passingham, R.E., Silbersweig, D., Ceballos-Baumann, A.O., Frith, C.D., Frackowiak, R.S., 1995. Functional anatomy of the mental representation of upper extremity movements in healthy subjects. *J. Neurophysiol.* 73, 373–386.
- Talairach, J., Tournoux, P., 1993. Referentially oriented cerebral MRI anatomy: an atlas of stereotaxic anatomical correlations for gray and white matter. Thieme.
- Tallon-Baudry, C., Bertrand, O., Delpuech, C., Pernier, J., 1996. Stimulus specificity of phase-locked and non-phase-locked 40 Hz visual responses in human. *J. Neurosci.* 16, 4240–4249.
- Tort, A.B.L., Komorowski, R., Eichenbaum, H., Kopell, N., 2010. Measuring phase-amplitude coupling between neuronal oscillations of different frequencies. *J. Neurophysiol.* 104, 1195–1210. <http://dx.doi.org/10.1152/jn.00106.2010>.
- van der Meij, R., Kahana, M., Maris, E., 2012. Phase-amplitude coupling in human electrocorticography is spatially distributed and phase diverse. *J. Neurosci.* 32, 111–123. <http://dx.doi.org/10.1523/JNEUROSCI.4816-11.2012>.
- VanRullen, R., Busch, N., Drewes, J., Dubois, J., 2011. Ongoing EEG phase as a trial-by-trial predictor of perceptual and attentional variability. *Front. Psychol.* 2, 60.
- Vidal, J.R., Freyermuth, S., Jerbi, K., Hamame, C.M., Ossandon, T., Bertrand, O., Minotti, L., Kahane, P., Berthoz, A., Lachaux, J.-P., 2012. Long-distance amplitude correlations in the high gamma band reveal segregation and integration within the reading network. *J. Neurosci.* 32, 6421–6434.
- Vidal, J.R., Perrone-Bertolotti, M., Levy, J., De Palma, L., Minotti, L., Kahane, P., Bertrand, O., Lutz, A., Jerbi, K., Lachaux, J.-P., 2014. Neural repetition suppression in ventral occipito-temporal cortex occurs during conscious and unconscious processing of frequent stimuli. *Neuroimage* 95, 129–135.
- Voytek, B., 2010. Shifts in gamma phase–amplitude coupling frequency from theta to alpha over posterior cortex during visual tasks. *Front. Hum. Neurosci.* 4. <http://dx.doi.org/10.3389/fnhum.2010.00191>.
- Voytek, B., D'Esposito, M., Crone, N., Knight, R.T., 2013. A method for event-related phase/amplitude coupling. *Neuroimage* 64, 416–424. <http://dx.doi.org/10.1016/j.neuroimage.2012.09.023>.
- Waldert, S., Pistohl, T., Braun, C., Ball, T., Aertsen, A., Mehring, C., 2009. A review on directional information in neural signals for brain-machine interfaces. *J. Physiol. Paris* 103, 244–254. <http://dx.doi.org/10.1016/j.jphysparis.2009.08.007>.
- Waldert, S., Preissl, H., Demandt, E., Braun, C., Birbaumer, N., Aertsen, A., Mehring, C., 2008. Hand movement direction decoded from MEG and EEG. *J. Neurosci.* 28, 1000–1008. <http://dx.doi.org/10.1523/JNEUROSCI.5171-07.2008>.
- Weaver, K.E., Wander, J.D., Ko, A.L., Casimo, K., Grabowski, T.J., Ojemann, J.G., Darvas, F., 2016. Directional patterns of cross frequency phase and amplitude coupling within the resting state mimic patterns of fMRI functional connectivity. *Neuroimage* 128, 238–251.
- Whittingstall, K., Logothetis, N.K., 2009. Frequency-band coupling in surface EEG reflects spiking activity in monkey visual cortex. *Neuron* 64, 281–289. <http://dx.doi.org/10.1016/j.neuron.2009.08.016>.
- Yanagisawa, T., Yamashita, O., Hirata, M., Kishima, H., Saitoh, Y., Goto, T., Yoshimine, T., Kamitani, Y., 2012. Regulation of motor representation by phase–amplitude coupling in the sensorimotor cortex. *J. Neurosci.* 32, 15467–15475. <http://dx.doi.org/10.1523/JNEUROSCI.2929-12.2012>.